Dalton Transactions

Accepted Manuscript

ROYAL SOCIETY OF CHEMISTRY

www.rsc.org/dalton

Lactide polymerization catalyzed by Mg and Zn diketiminate complexes with flexible ligand frameworks

*Todd J. J. Whitehorne, Boris Vabre, Frank Schaper**

Centre in Green Chemistry and Catalysis (CGCC), Département de chimie, Université de Montréal, 2900 Boul. E.-Montpetit, Montréal, QC, H3T 1J4, Canada

Diketimine ligands bearing *N*-benzyl, *N*-9-anthrylmethyl and *N*-mesitylmethyl substituents (*nacnac*^{Bn}H, *nacnac*^{An}H, and *nacnac*^{Mes}H) were prepared from condensation of the amine with either acetyl acetone or its ethylene glycol monoketal. Chlorination with *N*-chlorosuccinimide in the 3-position yielded Cl*nacnac*^{Bn}H and Cl*nacnac*^{An}H. The ligands were reacted with Zn(TMSA)$_2$ (TMSA = N(SiMe$_3$)$_2$) to yield *nacnac*^{An}Zn(TMSA) and Cl*nacnac*^{Bn}Zn(TMSA). Protonation with isopropanol afforded *nacnac*^{An}ZnO*i*Pr and Cl*nacnac*^{Bn}ZnO*i*Pr. Reaction of the diketimines with Mg(TMSA)$_2$ afforded *nacnac*^{An}Mg(TMSA), *nacnac*^{Mes}Mg(TMSA), Cl*nacnac*^{Bn}Mg(TMSA) and Cl*nacnac*^{An}Mg(TMSA). Subsequent protonation with *tert*-butanol produced *nacnac*^{Mes}MgO*t*Bu and Cl*nacnac*^{Bn}MgO*t*Bu, but only decomposition was observed with *N*-anthrylmethyl substituents. Most complexes were characterized by X-ray diffraction studies. TMSA complexes were monomeric, alkoxide complexes dimeric in the solid state. All alkoxide complexes, as well as *nacnac*^{An}Mg(TMSA)/BnOH and Cl*nacnac*^{An}Mg(TMSA)/BnOH were moderately to highly active in *rac*-lactide polymerization (90% conversion in 30 sec to 3 h). *nacnac*^{An}ZnO*i*Pr produced highly heterotactic polymer (P_r = 0.90), Cl*nacnac*^{Bn}MgO*t*Bu/BnOH produced slightly isotactic polymer at –30 °C (P_r = 0.43), all other catalysts produced atactic polymers with a slight heterotactic bias.

Introduction

Biodegradable polymers,[1-3] i. e. polymers which degrade completely into CO_2 and water in the environment, are gaining importance or at least interest due to concerns about the impact of macroscopic plastic debris and microplastics on wildlife,[4] in particular in the marine environment.[5-7] Polyesters are attractive targets for biodegradable polymers, since the ester bond can be cleaved by hydrolysis. Of these, polylactic acid (PLA), which is currently used in medical applications and produced on an industrial scale for packing applications, offers the additional advantage that the monomer is obtained from a renewable feedstock.[3, 8-10] PLA is obtained industrially from Sn-catalyzed polymerization of lactide, the dimeric anhydride of lactic acid. Catalyst development for the coordination-insertion polymerization of lactide has become a highly frequented research area due to the challenge of polymerizing lactide with high isotacticity and high activity.[8, 11-17] Compared to α-olefin polymerization, for example, general structure-reactivity/selectivity relationships for the polymerization of lactide and other cyclic esters are mostly lacking. We investigated in recent years the influence of general catalyst geometry on catalyst performance using structurally similar *N*-alkyl diketiminates (*nacnac*^{R}) as spectator ligands. Octahedral zirconium bisdiketiminate complexes, (±)-C_6H_{10}-(*nacnac*^{R})$_2$Zr(OEt)$_2$ (Scheme 1), showed by far the highest activity obtained with group 4 metal catalysts, but did not provide selectivity and were unsatisfactory catalysts due to transesterification side reactions and catalyst decomposition.[18] Square-planar copper diketiminate complexes, {*nacnac*^{R}$_2$Cu(μ-O*i*Pr)}$_2$ (Scheme 1), also showed extremely high activities, which were orders of magnitude above other Cu(II) catalysts, but showed no stereoselectivity.[19, 20] Contrary to the octahedral Zr catalyst, the Cu catalyst was highly stable, able to produce block-copolymers, did not undergo either transesterification reactions or chain-transfer even in the absence of monomer, and was suitable for immortal polymerization. Zn and Mg catalysts, **1-3** (Scheme 1), having the same *N*-alkyl diketimine ligands in a tetrahedral coordination geometry, displayed only moderate activity in comparison to other complexes with the same central metal.[21, 22] While the Zn catalysts provided heterotactic polymer, Mg catalyst **3**

showed a slight preference for isotactic monomer enchainment at low temperatures. The source of the preference for isotactic enchainment is not clear at the moment, but a ligand-mediated chain-end control mechanism was proposed based on the available data.[21]

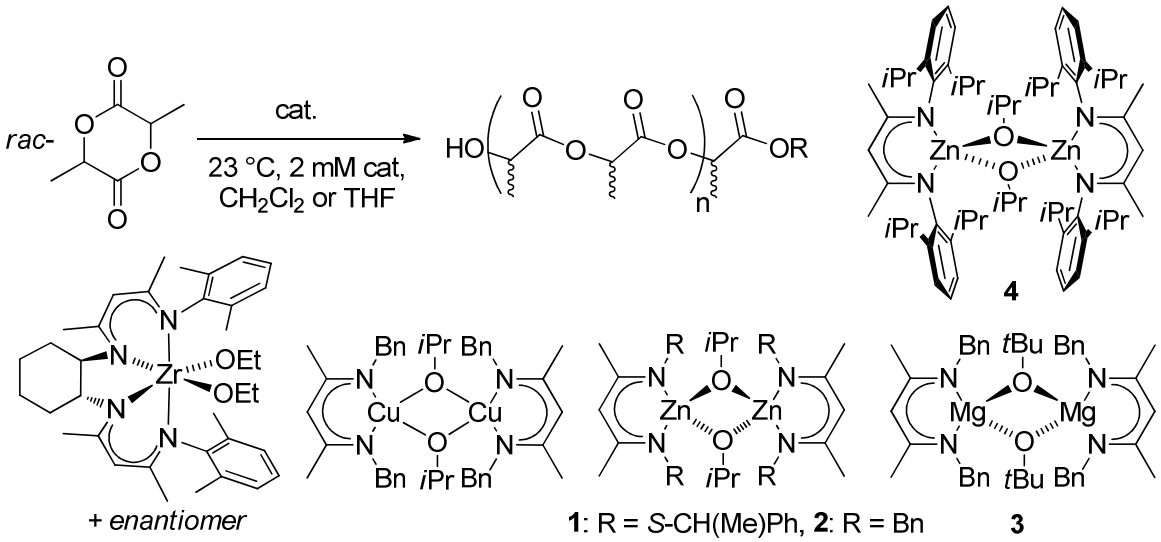

Scheme 1

Zinc[22-39] and magnesium[21, 24-31, 40-43] diketiminate complexes have been widely used in lactide polymerization, starting with the seminal work of Coates using *nacnac*^{dipp}ZnO*i*Pr,[44] **4**, (dipp = diisopropylphenyl).[23, 24] In all cases, monomer insertion occurred either unselectively or with heterotactic preference, following a chain-end control mechanism. The latter can be very efficient, provided that the ligand is sufficiently bulky, and P_r-values of >90% were be obtained with several catalysts (P_r = probability of alternating enantiomer insertion). Non-symmetric, mono-substituted *N*-aryl diketiminate ligands have been used in several cases to yield C_2- or C_1-symmetric Mg or Zn diketiminate complexes.[27-29, 37-39] However, catalyst geometry did not impact on stereoselectivity and the catalysts continued to show only heterotactic preference, if any, for monomer insertion in the polymerization of *rac*-lactide.[27-29, 37, 38] Complex **3** thus represents so far the only example of a diketiminate catalyst with an isotactic preference and only few magnesium complexes with other ligands systems have been reported to produced isotactically enriched PLA (P_r = 0.36,[45] 0.35 – 0.45,[46] and 0.30-0.41[47]). Herein we report further investigations into Mg and Zn diketiminate catalysts with

primary alkyl substituents on the nitrogen atoms to explore potential benefits of a flexible ligand framework.

Results and Discussion

Zinc complexes. Initial variations of the ligand substitution pattern concentrated on increasing the steric bulk of the *N*-benzyl substituent by replacement with *N*-anthrylmethyl (**5a**, Scheme 2). The condensation of anthrylmethylamine with acetyl acetone, a route successfully employed for other *N*-alkyl diketimines,[48] yielded only the monocondensation product (Scheme 2), regardless of reaction conditions (1-2 equiv HCl, TsOH or a mixture of both). Condensation in ethanolic HCl at reflux[49] likewise failed to provide **5a**. Reaction of acetyl acetone ethylene glycol monoketal (Scheme 2) with two equiv of amine in the absence of solvent[50, 51] finally yielded **5a** in 62% yield (see Fig. S1 for the crystal structure of **5a**).

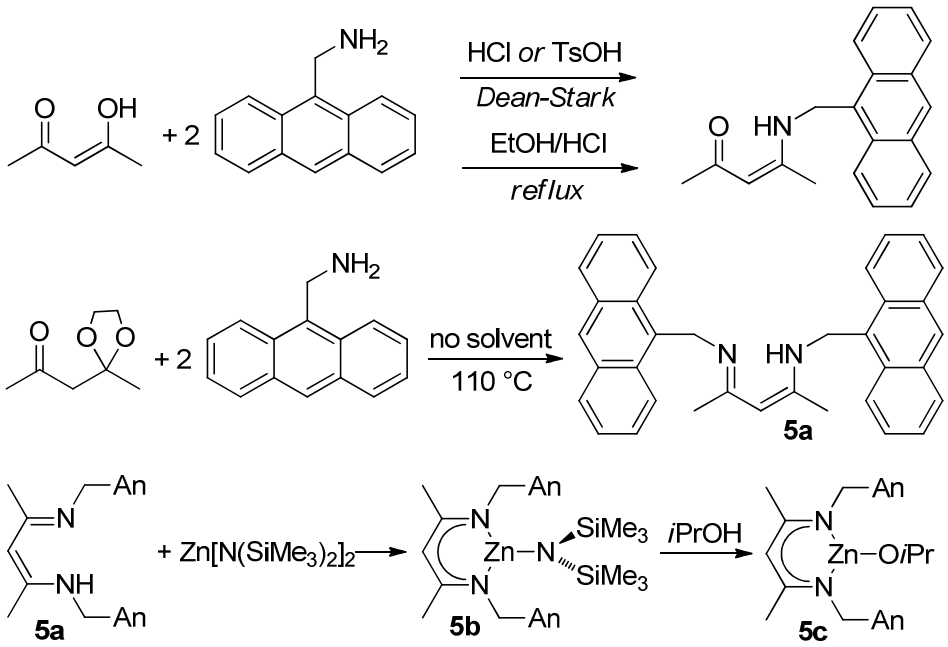

Scheme 2

Reaction of **5a** with $Zn[N(SiMe_3)_2]_2$ cleanly yielded the respective Zn amide complex, **5b** (Scheme 2). Further protonation with isopropanol afforded *nacnac*^{An}ZnO*i*Pr, **5c**. As typically observed for *nacnac*$ZnN(SiMe_3)_2$ complexes, **5b** crystallized as a monomeric complex with a trigonal-planar geometry around the Zn atom and a perpendicular orientation of the amide ligand versus the ligand

mean plane (Fig. 1). Bond distances and angles in **5b** are in the range typically observed for *nacnac*ZnN(SiMe$_3$)$_2$ (Table S1).[22, 28, 29, 52, 53] Alkoxide complex **5c** crystallized as an alkoxide bridged dimer (Fig. 2), as do all other similar complexes with the exception of monomeric *nacnac*^{dipp}ZnO*t*Bu.[26] The zinc atom is found in a distorted tetrahedral coordination geometry. Bond distances and angles are comparable to other alkoxide bridged zinc diketiminates (Table S1),[22-24, 39, 52, 54-57] but on the lower end of the range observed for Zn-N distances and the higher end for the N-Zn-N angle, indicating rather low steric pressure from the ligand despite the annulated aromatic ring. The orientation of the anthryl moieties in **5c** are in agreement with π-stacking interactions: the anthryl moieties are nearly coplanar (angle between mean planes: 7°), with a slight offset placing a carbon atom in the middle of the aromatic rings and distances of 3.3 – 3.7 Å.

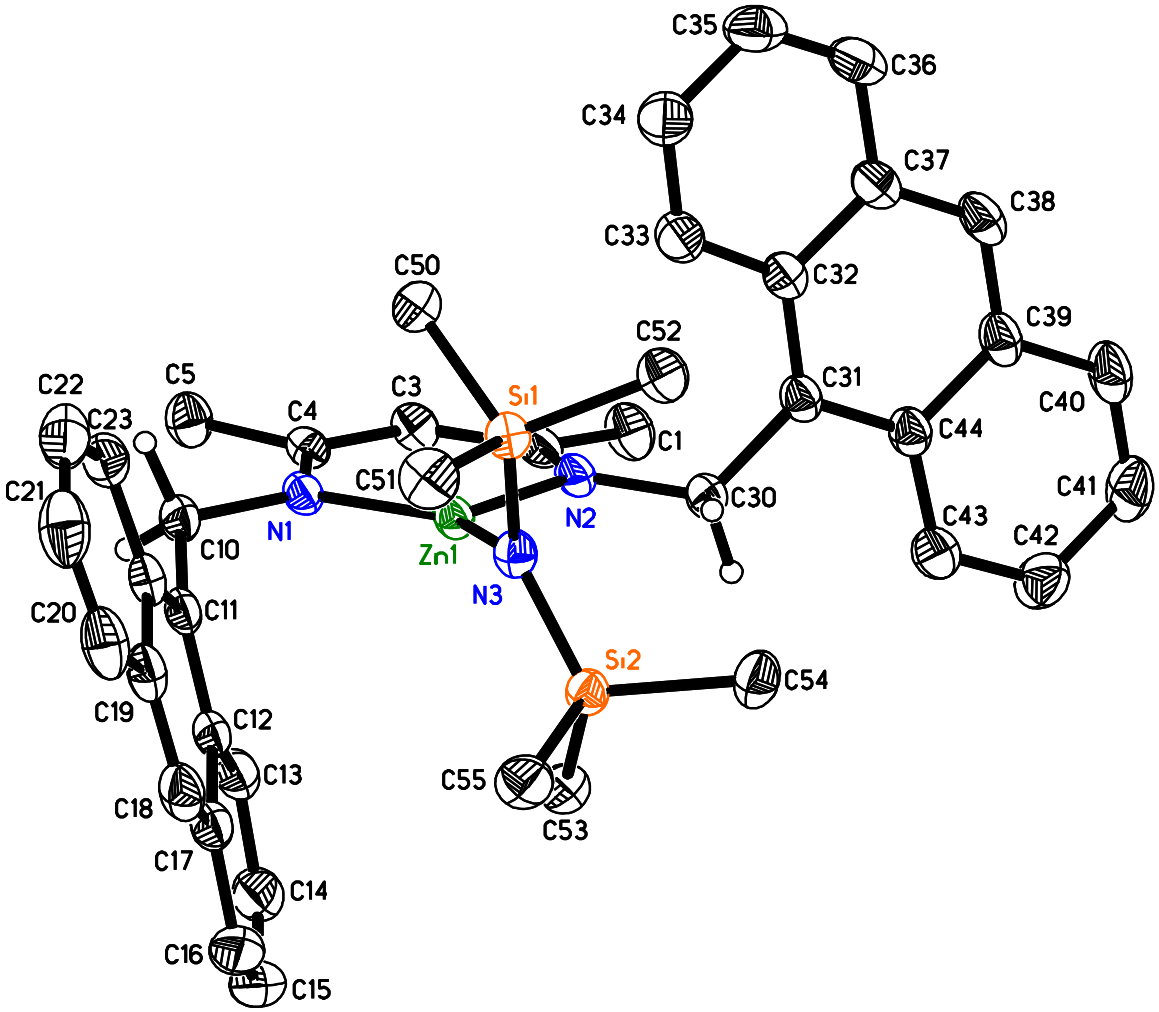

Fig. 1. X-ray structure of **5b**. Most hydrogen atoms, the second independent molecule of comparable geometry and co-crystallized solvent were omitted for clarity. Thermal ellipsoids are drawn at 50%

probability. Bond distances/Å: Zn1-N1: 1.935(1) & Zn2-N5: 1.935(1), Zn1-N2: 1.986(1) & Zn2-N4: 1.992(1), Zn1-N3: 1.897(1) & Zn2-N6: 1.902(1). Bond angles/deg: N1-Zn1-N2: 100.11(6) & N4-Zn2-N5: 99.60(6), N1-Zn1-N3: 142.41(6) & N5-Zn2-N6: 144.00(6), N2-Zn1-N3: 117.30(6) & N4-Zn2-N6: 116.33(6).

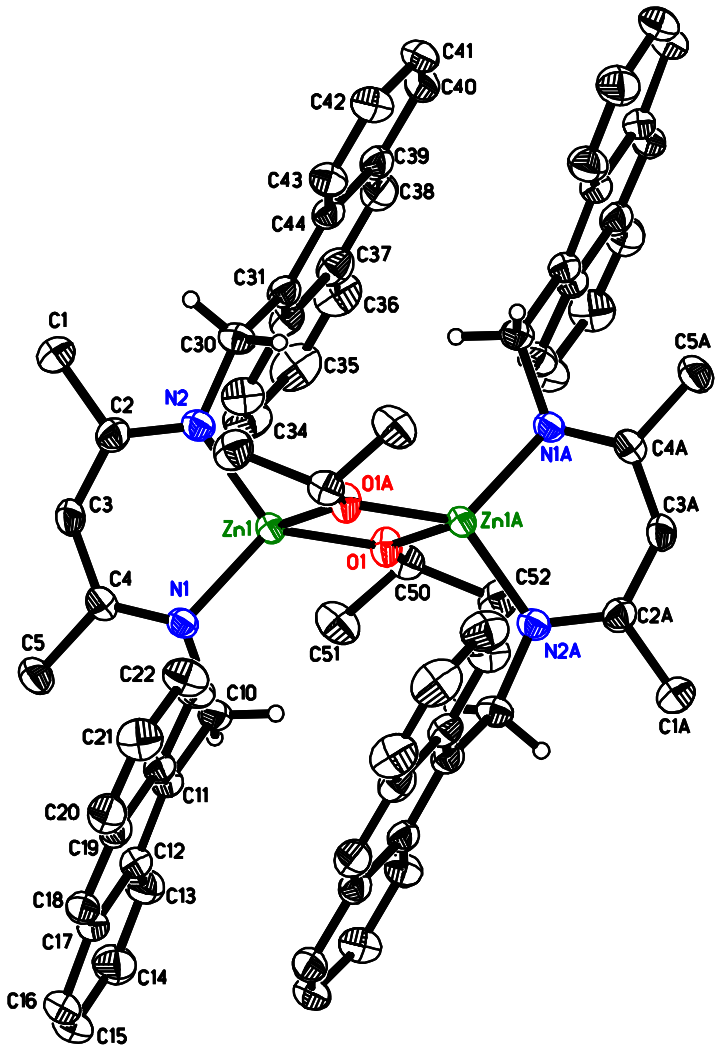

Fig. 2. X-ray structure of **5c**. Most hydrogen atoms and co-crystallized solvent omitted for clarity. Thermal ellipsoids are drawn at 50% probability. The molecule has crystallographic inversion symmetry. Bond distances/Å: Zn1-N1: 1.972(2), Zn1-N2: 1.959(2), Zn1-O1: 1.975(2), Zn1-O1A: 1.976(2), Zn1-Zn1A: 2.982(1). Bond angles/deg: N1-Zn1-N2: 100.65(7), O1-Zn1-O1A: 82.01(6), N1-Zn1-O1: 117.76(7), N2-Zn1-O1: 121.15(7), N1-Zn1-O1A: 126.23(7), N2-Zn1-O1A: 110.25(7), Zn1-O1-Zn1A: 97.99(6).

Complex **5c** proved to be a moderately active and controlled catalyst for the solution polymerization of *rac*-lactide (Table 1, Fig. S2). After a short induction period, the reaction was first-order in lactide concentration with an apparent rate constant of k_{app} = $1.2 \cdot 10^{-2}$ – $1.6 \cdot 10^{-2}$ min^{-1} at 2 mM catalyst concentration. The activity is very similar to the rate constants observed for the respective *N*-benzyl complex **1** (k_{app} = $2 \cdot 10^{-2}$ - $4 \cdot 10^{-2}$ min^{-1}) and *N*-methylbenzyl complex **2** (k_{app} = $1 \cdot 10^{-2}$ - $2 \cdot 10^{-2}$ min^{-1})[22] and only slightly lower than *nacnac*^{dipp}ZnO*i*Pr, **4** (k_{app} = $5 \cdot 10^{-2}$ min^{-1}).[24] The obtained polymer is highly heterotactic, with P_r values around 90% (Table 1, P_r). Complex **5c** thus shows an even higher heterotactic preference then the corresponding benzyl complex **2**. A closer look at the crystal structures of **5b** and **5c** offers a tentative explanation for the lack of catalytic-site control. In **5b**, one anthrylmethyl substituent is oriented nearly symmetrically with regard to the ligand mean plane (Fig. 1), the other is turned with the anthryl moiety towards the backbone of the ligand. The latter orientation is also observed for one of the *N*-substituents in dimeric **5c** (Fig. 2). In both orientations, complex geometry becomes essentially C_S-symmetric and no catalytic site control by a putative C_2-symmetric rotamer is observed. Polymer molecular weight control with **5c** was rather poor and polymer molecular weights significantly higher than expected were obtained. Neither a notable induction period nor catalyst decomposition was observed, in agreement with overall narrow polydispersities. Prolonged reaction times after completion of polymerization increased the P_r value as well as the discrepancy between expected and obtained polymer molecular weight (c. f. #1 vs. #2). This might indicate transesterification side-reactions as possible source for the lack of polymer molecular weight control (see supp. information).[22] In the presence of one equiv of benzyl alcohol, the expected molecular weight for two chains per metal center is obtained with narrow polydispersities (Table 1, #3), indicating some stability of **5c** under immortal polymerization conditions. Zinc (and magnesium) diketiminate complexes with *N*-alkyl substituents are, however, generally labile towards ligand protonation by excess alcohol.

Table 1 *Rac*-Lactide polymerization with Zn complexes

#	Catalyst	[Zn] : lactide (: BnOH)	Conversion / time	Final conversion	P_r [a]	M_n [b] ·mol/g	Chains per Zn [c]	M_w/M_n
1	**5c**	1:300	40% / 30 min	93% / 3 h	0.88	66 500	0.6	1.14
2	**5c**	1:300	33% / 30 min	95% / 6 h	0.93	118 000	0.3	1.16
3	**5c**	1:300:1	19% / 30 min	87% / 3 h	0.87	14 900	2.3	1.04
4	**6c**	1:300	80% / 3h	80%	0.59	n. d.		

Conditions: CH_2Cl_2, ambient temperature (23 °C), 2 mM [Zn]. Conversion determined from ^{1}H NMR. [a] P_r determined from decoupled ^{1}H NMR by $P_r = 2{\cdot}I_1/(I_1+I_2)$, with I_1 = 5.20 – 5.25 ppm (*rmr, mmr/rmm*), I_2 = 5.13 – 5.20 ppm (*mmr/rmm, mmm, mrm*). [b] M_w and M_n determined by size exclusion chromatography vs. polystyrene standards, with an MH correction factor of 0.58. Number of chains per catalyst determined from (conversion$\cdot m_{lactide}/n_{Zn}+M_{i\mathrm{PrOH}})/M_n$.[c]

To investigate electronic effects on catalyst performance, we prepared diketimine **6a** with a chlorine substituent in the 3-position of the ligand backbone by reaction of the parent diketimine with *N*-chlorosuccinimide (Scheme 3). Reaction with $Zn[N(SiMe_3)_2]_2$ yielded the amide complex **6b** as an oil, which was reacted, without further purification, with isopropanol to yield alkoxide complex **6c**. Polymerisation of *rac*-lactide with **6c** (Table 1, #4) showed an activity comparable to that of its non-chlorinated analogue **2** and a P_r value of 0.59, only slightly reduced compared to **2** (0.65 – 0.71).[22]

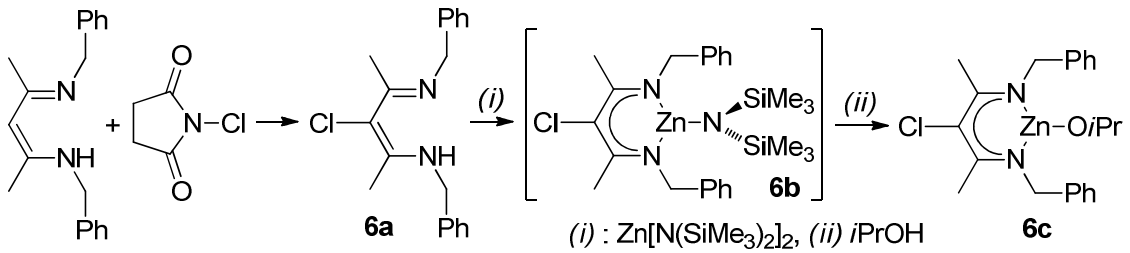

Scheme 3

Magnesium complexes. Since magnesium complex **3** was the first diketiminate complex with an isotactic preference for monomer insertion, it was of interest to see how slight variations of the substitution pattern influenced stereoselectivity in lactide polymerization. Reaction of $Mg[N(SiMe_3)_2]_2$ with **5a** yielded the respective amide complex **5d** (Scheme 4). As other diketiminate metal amides, **5d** is monomeric in the solid state (Fig. 3). In comparison to the corresponding Zn amide **5b** (Fig. 1), the

more ionic bonds in the Mg complex allow a stronger deviation from trigonal-planar geometry and the Mg atom is bent by 29° out of the plane of the diketiminate ligand. This deviation is higher than in the corresponding *N*-aryl complex *nacnac*^{dipp}MgN(SiMe$_3$)$_2$,[58] where this deviation is only 16°. The difference can be ascribed to the higher flexibility of *N*-alkyl diketiminates, which allow an easier out-of-plane bending of the metal atom.[59] Other geometrical parameters in **5d** are comparable to those of *nacnac*^{dipp}MgN(SiMe$_3$)$_2$ (Table S2).

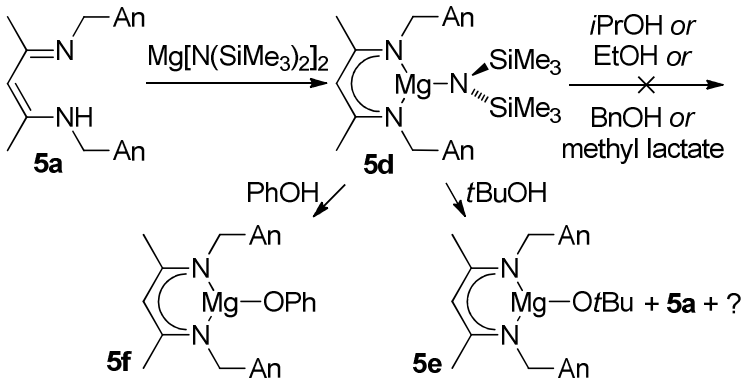

Scheme 4

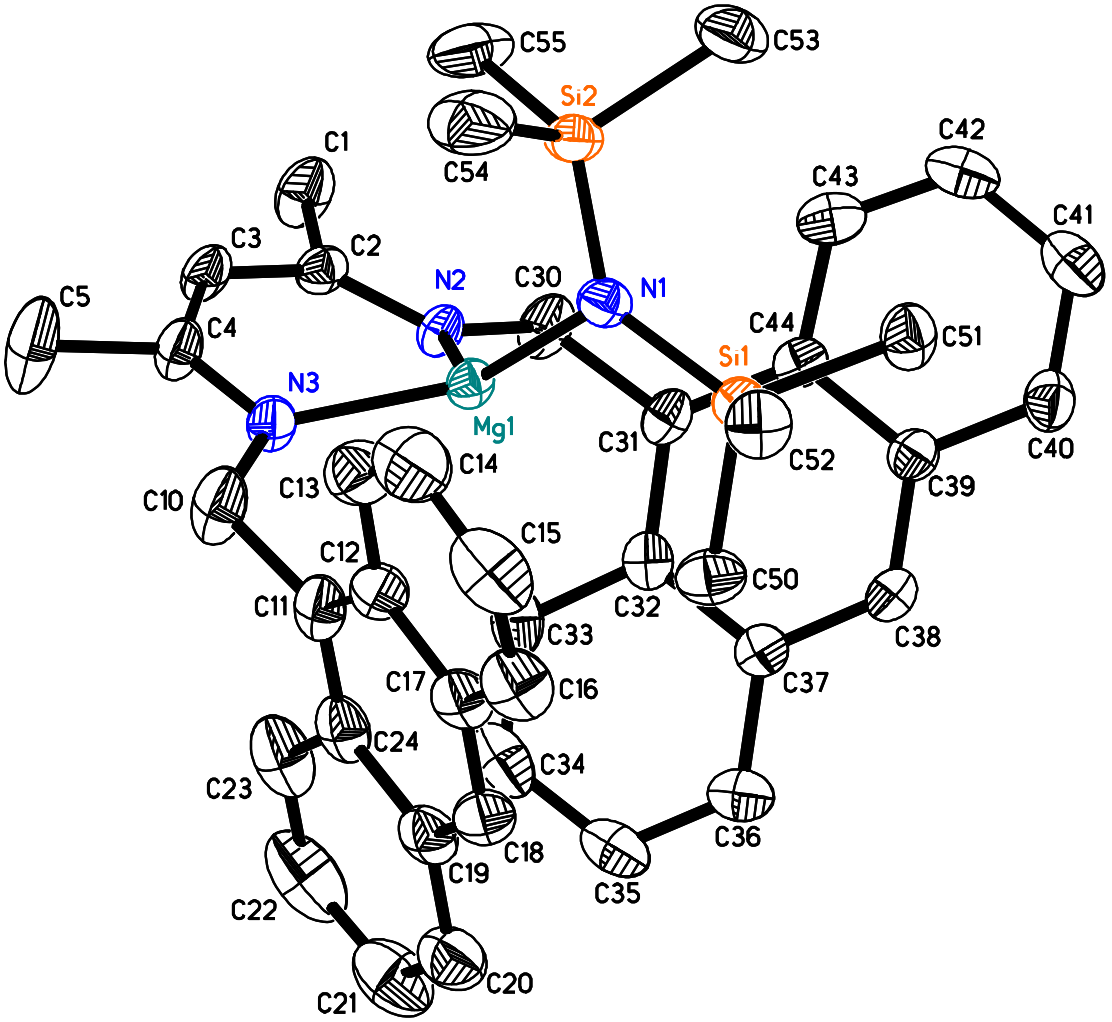

Fig. 3. X-ray structure of **5d**. Hydrogen atoms and co-crystallized solvent omitted for clarity. Thermal ellipsoids are drawn at 50% probability. Mg1-N2: 2.026(2) Å, Mg1-N3: 2.029(2) Å, Mg1-N1: 1.972(2) Å, N2-Mg1-N3: 96.80(8)°, N1-Mg1-N2: 126.55(8)°, N1-Mg1-N3: 125.34(9)°.

Attempts to introduce an alkoxide substituent by reaction of **5d** with isopropanol led to decomposition. In the case of **3**, similar problems had been circumvented by employing *tert*-butanol,[21] but the reaction proved less controlled with **5d**: When an C_6D_6 solution of **5d** was titrated with *tert*-butanol, resonances assigned to the target complex **5e** were obtained upon addition of 0.25 equiv of *tert*-butanol (Scheme 4, Fig. S3). Further addition of alcohol, however, led to the presence of increasing amounts of the ligand **5a** and unknown by-products. (The expected by-product, homoleptic $(nacnac^{An})_2Mg$, seems not to be present in the mixture. Likewise, we were unable to prepare the homoleptic complex by reaction of magnesium amide with two equiv of **5a**.) Although

tert-butoxide complex **5e** was the major species present, we were unable to obtain a pure product despite extensive recrystallisation experiments. Reaction of **5d** with several other alcohols, such as ethanol, benzyl alcohol, methyl lactate, or phenol, likewise failed to yield an isolatable pure product. In the case of phenol, single crystals of the phenolate complex **5f** suitable for X-ray diffraction were obtained (Fig. 4), but only in quantities insufficient for further characterization. Bond distances and angles in **5f** are comparable to other [*nacnac*Mg(μ-OR)]$_2$ complexes (Table S3).[21, 24, 29, 60] The structure of **5f** illustrates the high flexibility of *N*-alkyl diketiminate ligands: all the anthryl orientations described for **5b** and **5c** are realized in **5f**. Two anthryl groups are arranged in a π-stacking orientation and display the forward orientation of the anthryl moiety targeted for effective stereocontrol, the other two do not show suitable orientations for enforcing C_2-symmetry: one anthryl group is nearly perpendicular to the mean ligand plane, the other one is rotated towards the ligand backbone.

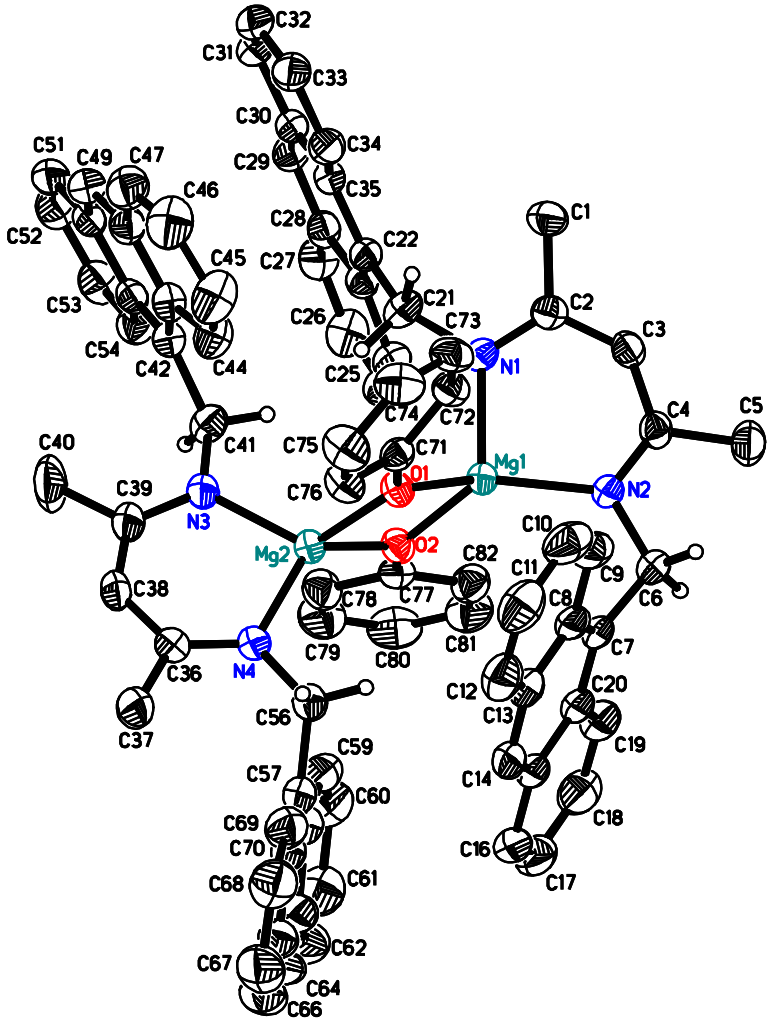

Fig. 4. X-ray structure of **5f**. Most hydrogen atoms and co-crystallized solvent omitted for clarity. Thermal ellipsoids are drawn at 50% probability. Bond distances/Å: Mg1-N1: 2.0559(15), Mg1-N2: 2.0406(15), Mg2-N3: 2.0281(16), Mg2-N4: 2.0172(16), Mg1-O1: 1.9862(13), Mg1-O2: 1.9940(13), Mg2-O1: 1.9700(13), Mg2-O2: 1.9845(13), Mg1-Mg2: 3.0122(8). Bond angles/deg: N1-Mg1-N2: 94.88(6), N3-Mg2-N4: 95.67(6), O1-Mg1-O2: 80.65(5), O1-Mg2-O2: 81.29(5).

In the absence of an isolated alkoxide complex, the amide complex **5d** was employed for *rac*-lactide polymerizations. Surprisingly, **5d** proved to be highly active (Table 2, #1; Fig. S4), slightly faster than complex **3** with *N*-benzyl substituents. None of the polymerizations performed reached completion, indicating instability of the catalyst under polymerization conditions. As with **3**, polymerization at room temperature yielded an atactic polymer. A notable induction period (Fig. S4), a low number of polymer chains per catalyst center and high polydispersities above 1.8 indicate slow initiation of polymerization. Addition of one equiv benzyl alcohol to polymerizations with **5d** removed the induction period and polymerization was complete in less than one minute (Table 2, #2-#8; Fig. S5+S6; c.f.: *nacnac*^{dipp}MgOR, 97% in 2 min[24]), rendering **5d** a highly active catalyst with k_{obs} = 2.8(3) min^{-1} at 2 mM catalyst concentration. If two equiv BnOH were used (Table 2, #5; Fig. S5) or at an increased lactide:Mg ratio of 900:1 (Table 2, #8; Fig. S6), catalyst decomposition prevented complete polymerization. In all cases, the obtained polymer was atactic and, contrary to **3**, polymerization at reduced temperatures did not affect stereoselectivity (Table 2, #9). Polydispersities varied between 1.2 and 1.7, narrower than for polymerizations without additional alcohol, but nevertheless indicative of poor polymer weight control. In addition, obtained polymer weights were now much lower than expected with 1.5 to 3.9 polymer chains produced per metal center. Participation of $(Me_3Si)_2NH$ as a chain-transfer agent seems unlikely, given its low acidity and slow insertion rates. Consequently, no notable presence of polymer bound $N(SiMe_3)_2$ was detected in ^{1}H NMR spectra of polymers obtained with **5d**/BnOH. Variations in the catalyst:monomer ratio (1:100 – 1:900; #3, #6-#8) did not correlate with the number of polymer chains obtained per catalyst, thus excluding impurities in the monomer

acting as chain-transfer agents. Increasing amounts of benzyl alcohol (0.7 – 2 equiv; #2-#5), led to narrower polydispersities, in agreement with its activating effect on initiation, but they still remained above 1.15. Higher amounts of alcohol increased, as expected, the number of chains per catalyst center, but the obtained polymer molecular weight remained lower than expected in all cases. GPC traces did not indicate the presence of a low-molecular-weight fraction that would be indicative of intramolecular transesterifications to yield cyclic oligomers. However, the P_r value correlates – somewhat noisily – with the discrepancy of expected and obtained molecular weight, i. e. the number of chains per catalyst center produced (Fig. S7). Since a likely cause for variations in P_r are transesterification reactions (the appearance of rr-triads causes an artificial reduction of P_r, if calculated as described in Table 2), the observed discrepancy in expected and obtained molecular weight might be attributed to transesterification (see supp. inform.).

Table 2 *Rac*-Lactide polymerization with Mg catalysts

#	Catalyst	[Mg] : lactide (: BnOH)	Conversion / time	Final conversion	P_r [a]	M_n · mol/g [b]	Chains per Mg [b]	M_w/M_n
1	**5d**	1:100	20 – 30% / 1 min [c]	60% – 65% [c]	0.51 – 0.52	15 100 – 15 700	0.6	1.79 – 1.87
2	**5d**	1:300:0.7	80% / 30 sec	95%	0.52	24 800	1.6	1.65
3	**5d**	1:300:1	75 - 95% / 30 sec [c]	> 95%	0.49	15 500 – 16 300	2.5 – 2.7	1.39 – 1.60
4	**5d**	1:300:1.3	95% / 30 sec	95%	0.49	13 300	3.1	1.49
5	**5d**	1:300:2	50% / 30 sec	70%	0.48	7900	3.9	1.15
6	**5d**	1:100:1	90% / 30 sec	95%	0.51	9500	1.4	1.29
7	**5d**	1:600:1	95% / 30 sec	> 95%	0.49	27 200	3.1	1.60
8	**5d**	1:900:1	60% / 30 sec	65%	0.50	36 800	2.2	1.45
9	**5d**, –30 °C	1:100:1		85% / 40 min	0.52	n. d.		
10	**7e**	1:300	70% / 5 min	80%	0.53	45 400	0.8	1.62
11	**7e**, –30 °C	1:300		92% / 17 h	0.55	55 500	0.7	1.98
12	**6e**	1:300	70 – 80% / 10 min [c]	75 – 90% [c]	0.53 – 0.57 [d]	23 300 – 39 000	0.8 – 1.6	1.34 – 1.71
13	**6e**	1:300:1	15 - 95% / 10 min [c]	30 – 95% [c]	0.49 – 0.53 [d]	16 600 – 27 800	0.7 – 2.1	1.04 – 1.20
14	**6e**, –30 °C	1:300:1		90-99% / 50 min [c]	0.43 [d]	31 900 – 37 900	1.1 – 1.2	1.08 – 1.11
15	**8d**	1:300:1	30% / 1 min	40%	0.48	n. d.		

Conditions: CH_2Cl_2, ambient temperature, 2 mM catalyst concentration. Final conversion without a given time is the maximum conversion, when the conversion/time plot plateaued. See supp. information for approximate rate constants. [a] P_r determined from decoupled ^{1}H NMR by $P_r = 2{\cdot}I_1/(I_1+I_2)$, with I_1 = 5.20 – 5.25 ppm (*rmr, mmr/rmm*), I_2 = 5.13 – 5.20 ppm (*mmr/rmm, mmm, mrm*). [b] M_n and M_w determined by size exclusion chromatography vs. polystyrene standards, with an MH correction factor of 0.58. Number of chains per Mg center determined from (conversion·$m_{lactide}/n_{Mg}+M_{i\text{PrOH}}$)/$M_n$. [c] Minimum and maximum values of multiple experiments. [d] From multiple aliquots/polymerizations (see

supporting information).

Given the high amount of π-stacking observed in the X-ray structures of **5c** and **5f**, which might stabilize the undesired *meso*-rotamer, we investigated ligand **7a**, which is sterically similar to **5a**, but should show a reduced tendency for π-π-interactions. Ligand **7a** was obtained similarly to **5a**, but the presence of molecular sieves was essential to obtain yields above 20% (Scheme 5). Reaction with $Mg[N(SiMe_3)_2]_2$ yielded the amide complex **7d**. The crystal structure of amide complex **7d** is nearly identical to that of **5d** (Fig. 5, Table S2) with the only difference being that the near C_s-symmetry in **5d** was observed as crystallographic C_s-symmetry in **7d**. Complex **7d** reacted with *tert*-butanol to yield **7e**. Alternatively, direct addition of *tert*-butanol to the crude reaction mixture containing **7d** in a one-pot, two-step reaction yielded **7e** in comparable yields. The crystal structure of **7e** shows a higher than usual bending of the Mg atom out of the mean plane of the diketiminate ligand and a likewise higher distortion from tetrahedral symmetry, which are both indicative of the steric strain introduced by the mesitylmethyl substituent, but otherwise geometric parameters are comparable to **5f**, **6e** and other dimeric $\{nacnacMg(\mu\text{-}OR)\}_2$ complexes (Fig. 6, Table S3).[21, 24, 29, 60] Satisfyingly, the π-stacking interactions observed in **5f** are absent in **7e**.

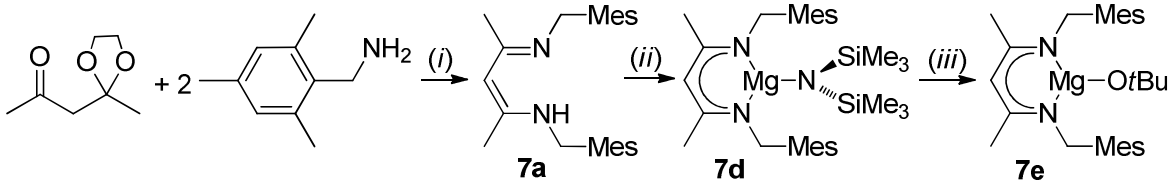

Mes = 2,4,6-trimethylphenyl. *(i)* : no solvent, Δ, mol. sieves, (*ii*): $Mg[N(SiMe_3)_2]_2$, *(iii)* *t*BuOH

Scheme 5

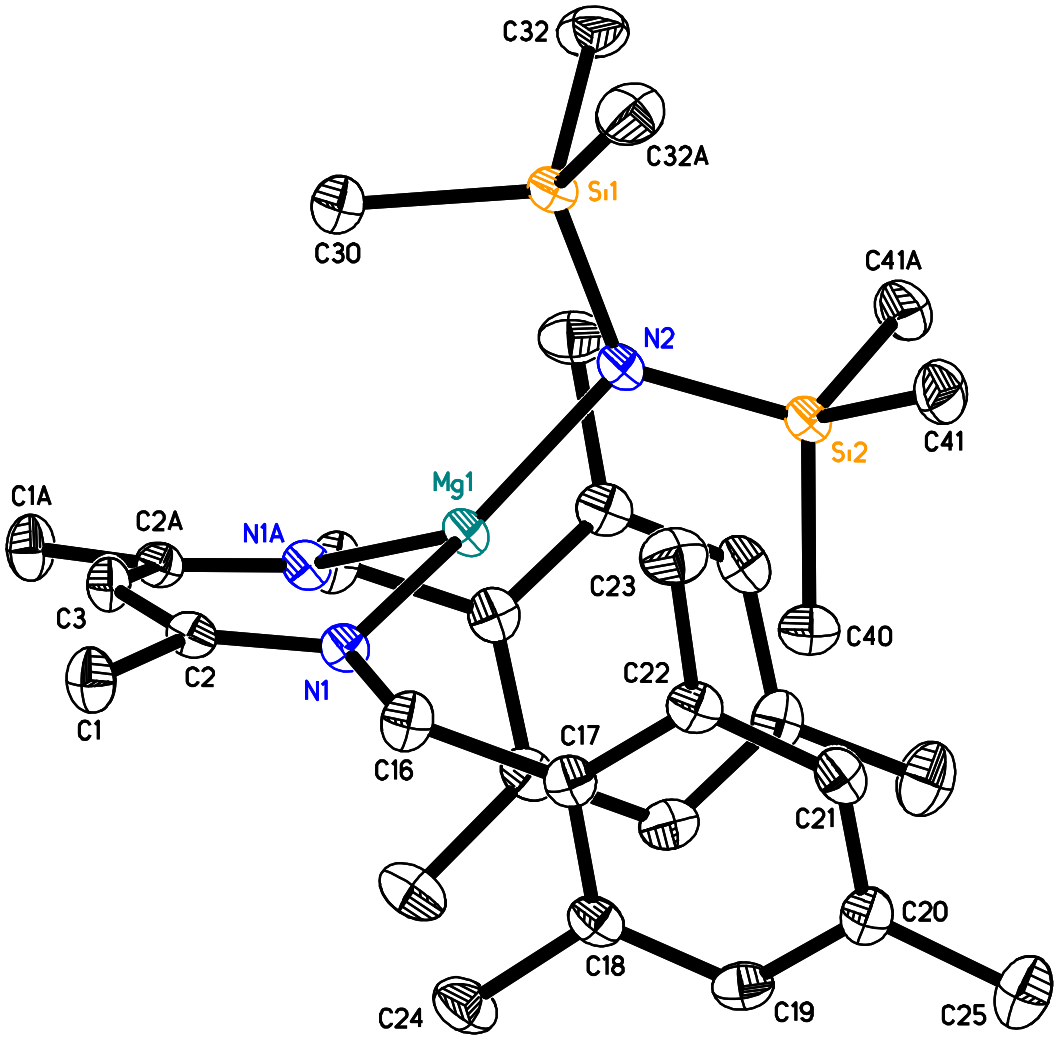

Fig. 5. X-ray structure of **7d**. Hydrogen atoms omitted for clarity. Thermal ellipsoids are drawn at 50% probability. Mg1-N1: 2.036(1) Å, Mg1-N2: 1.975(2) Å, N1-Mg1-N1A: 95.28(6)°, N1-Mg1-N2: 129.39(3)°.

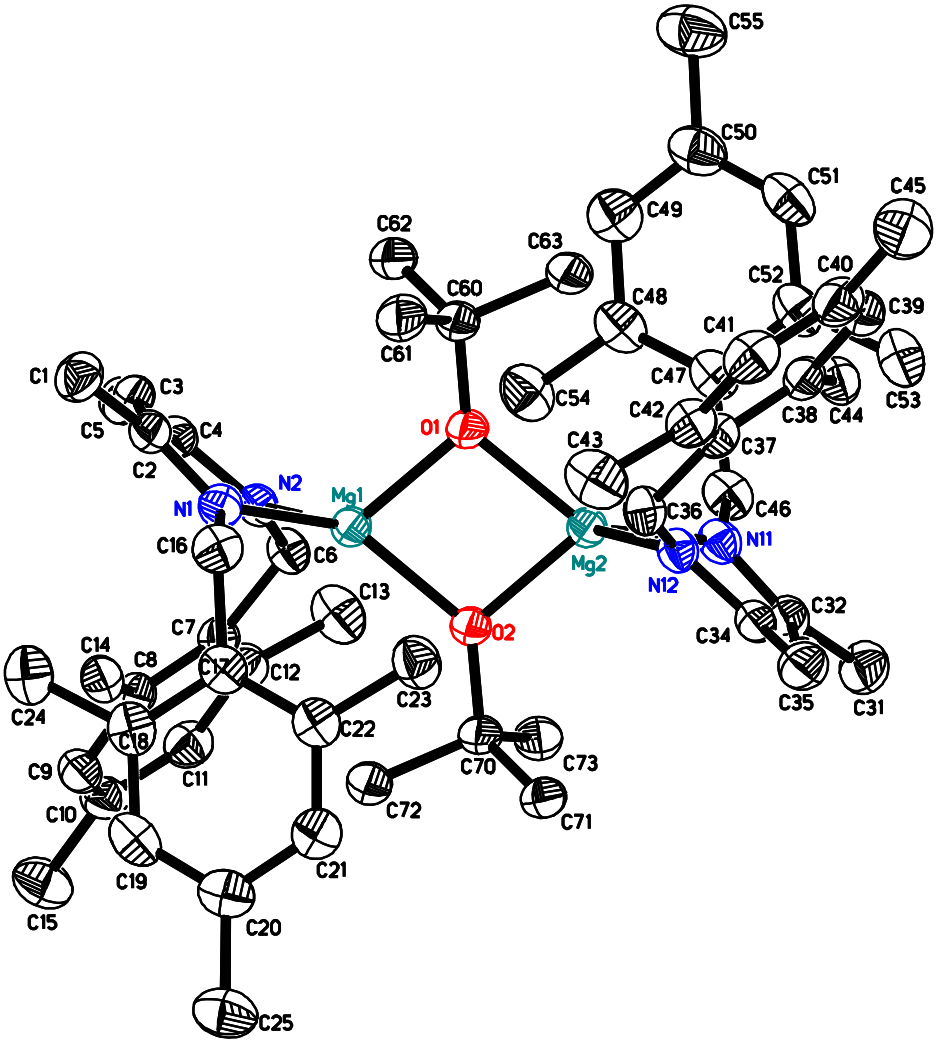

Fig. 6. X-ray structure of **7e**. Hydrogen atoms and co-crystallized solvent omitted for clarity. Thermal ellipsoids are drawn at 50% probability. Bond distances/Å: Mg1-N1: 2.0720(18), Mg1-N2: 2.0476(17), Mg2-N11: 2.0664(17), Mg2-N12: 2.0460(17), Mg1-O1: 1.9747(14), Mg1-O2: 1.9611(14), Mg2-O1: 1.9585(14), Mg2-O2: 1.9842(14), Mg1-Mg2: 2.9710(9). Bond angles/deg: N1-Mg1-N2: 90.57(7), N11-Mg2-N12: 90.96(7), O1-Mg1-O2: 82.18(6), O1-Mg2-O2: 82.00(6).

Performance of **7e** in lactide polymerization was disappointing (Table 2, #10-#11). Activities are lower than those of **5d**/BnOH, but are still significantly higher than those observed for **3**.[21] *Ortho*-substitution of the *N*-benzyl substituent thus increased activity in **7e** as well as **5d**. However, catalyst decomposition led to incomplete monomer consumption at room temperature and polydispersities were above 1.6 at room temperature and at –30 °C, despite a very minor induction period (Fig. S8). In addition, the catalyst showed no preference for isotactic monomer insertion even at low temperatures.

Magnesium complexes with β-chloro-diketiminate ligands. The effect of ligand chlorination was studied using β-chloro-diketimines **6a** and **8a** (Scheme 6). Reaction of $Mg[N(SiMe_3)_2]_2$ with **6a** yielded mixtures of $Mg[N(SiMe_3)_2]_2$, the heteroleptic amide complex **6d** and the homoleptic bisdiketiminate complex **6f**. To corroborate assignment, **6f** was prepared independently and characterized by X-ray diffraction (Fig. 7). Comparison of **6f** with the corresponding homoleptic complex lacking the chlorine substituent, *nacnac*$^{Bn}_2$Mg,[21] allows the delineation of the structural impact of introducing a substituent on the C_β atom of the diketiminate ligand (Table 3). Both structures show a distorted tetrahedral geometry, with similar orientations of the benzyl substituents. Electronic influences are rather small, leading to a minor contraction of the Mg-N bond lengths in **6f** (0.1 Å, Table 3). More notable is the steric impact of the chlorine substituent. By way of the methyl groups at the ligand backbone (widening of the C_β-C_α-C_{Me} angles by 3 – 4°, Table 3), substitution at C_β pushes the *N*-substituents closer to the front of the complex (reduction of C_N-C_β-C_N by 4° and of N-C_β-N by 2°). Other geometric data is consistent with a minor increase of steric pressure in **6f** (Table 3), in particular the slight reduction of the distances between Mg and the *N*-substituents.

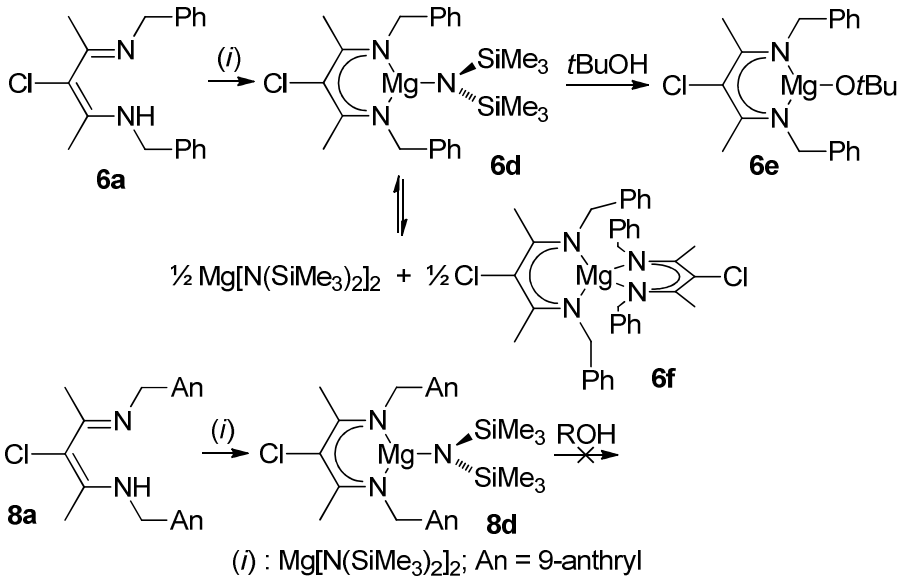

Scheme 6

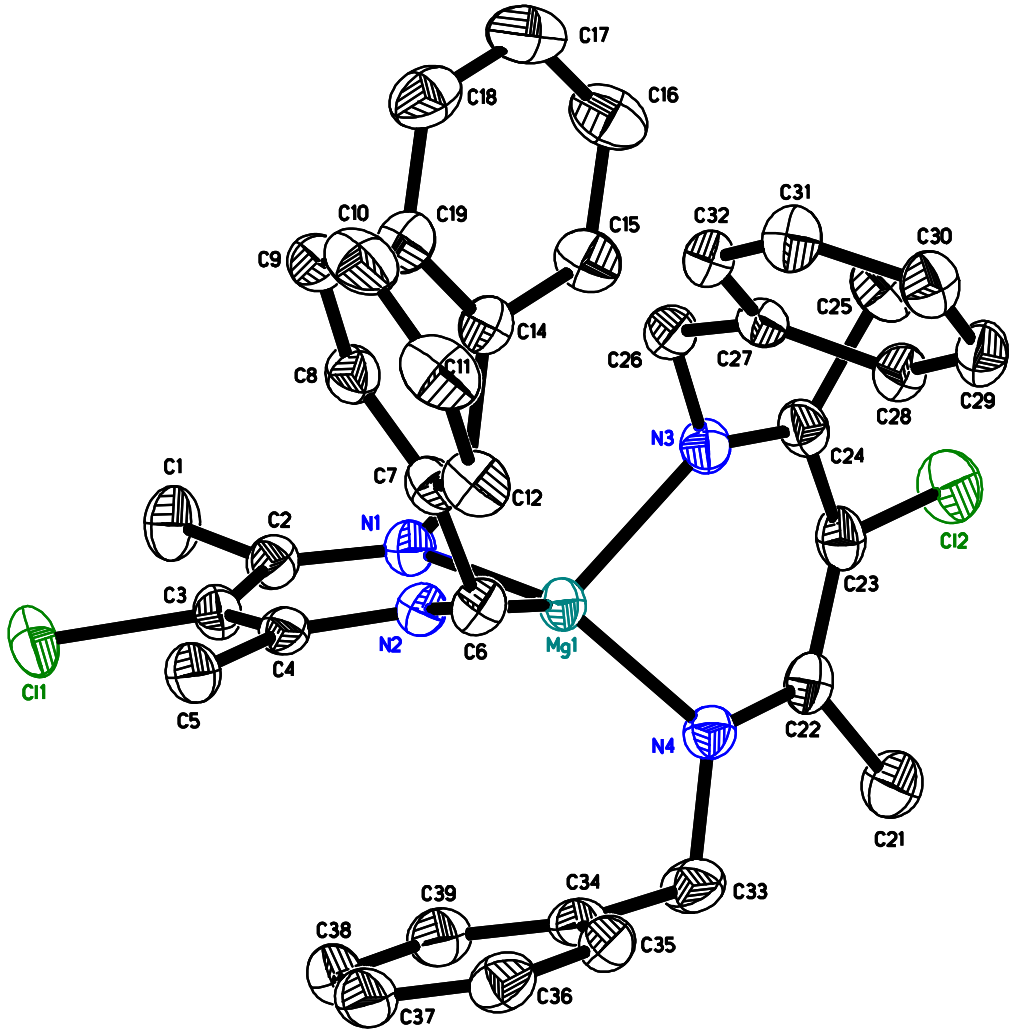

Fig. 7. X-ray structure of **6f**. Hydrogen atoms omitted for clarity. Thermal ellipsoids are drawn at 50% probability. Mg1-N1: 2.023(1) Å, Mg1-N2: 2.024(1) Å, Mg1-N3: 2.038(1) Å, Mg1-N4: 2.045(1) Å, N1-Mg1-N2: 90.39(5)°, N3-Mg1-N4: 89.93(5)°.

Table 3 Geometric impact of a chlorine substituent at the diketiminate C_β atom

	6f	**8f**	(*nacnac*^{Bn})$_2$Mg [21]	**6e**	**3** [21]
Mg-N	2.03(1) Å	2.07(1) Å	2.04(1) Å	2.037(2) Å	2.041(3)
Mg-C_N	2.98(6) Å	3.05(5) Å	3.02(2) Å	2.95 Å	3.01 – 3.06 Å
C_β-C_α-C_{Me}	118° – 119°	117° – 119°	114° – 116°	118°	115°
N-Mg-N	90°	88°	94°	92°	94°
C_N-C_β-C_N	95° – 96°	97° – 98°	100°	97°	99°
N-C_β-N	74°	73° – 74°	76°	75°	76°

Errors are standard deviations of the average of equivalent bond lengths or angles, not experimental uncertainties. C_N: benzylic carbon atom; C_β: central carbon atom of the ligand backbone; C_{Me}: diketiminate methyl group

Although heteroleptic **6d** could not be isolated from the obtained product mixtures, use of excess Mg[N(SiMe$_3$)$_2$]$_2$ favoured its formation sufficiently for NMR characterization. The alkoxide complex **6e** was obtained by addition of *tert*-butanol to a 1:1 mixture of **6a** and Mg[N(SiMe$_3$)$_2$]$_2$. The crystal structure of **6e** shows the expected dimeric structure with the Mg atom in a tetrahedral environment (Fig. 8). Contrary to its non-chlorinated analog **3**,[21] the *meso*-rotamer is observed in the solid state, with both *N*-benzyl substituents on the same side of the ligand plane. The *syn*-orientation of the benzyl substituents results in a smaller distortion of the tetrahedral coordination geometry around Mg than in **3**, where the benzyl groups are found in the *anti*-orientation of the C_2-symmetric rotamer (angle of the MgN_2 and MgO_2 mean planes: **6e**: 87°, **3**: 80°). In other aspects, **6e** is very similar to **3**, with the same minor steric impact of the chlorine substituent as discussed for **6f** (Table 3).

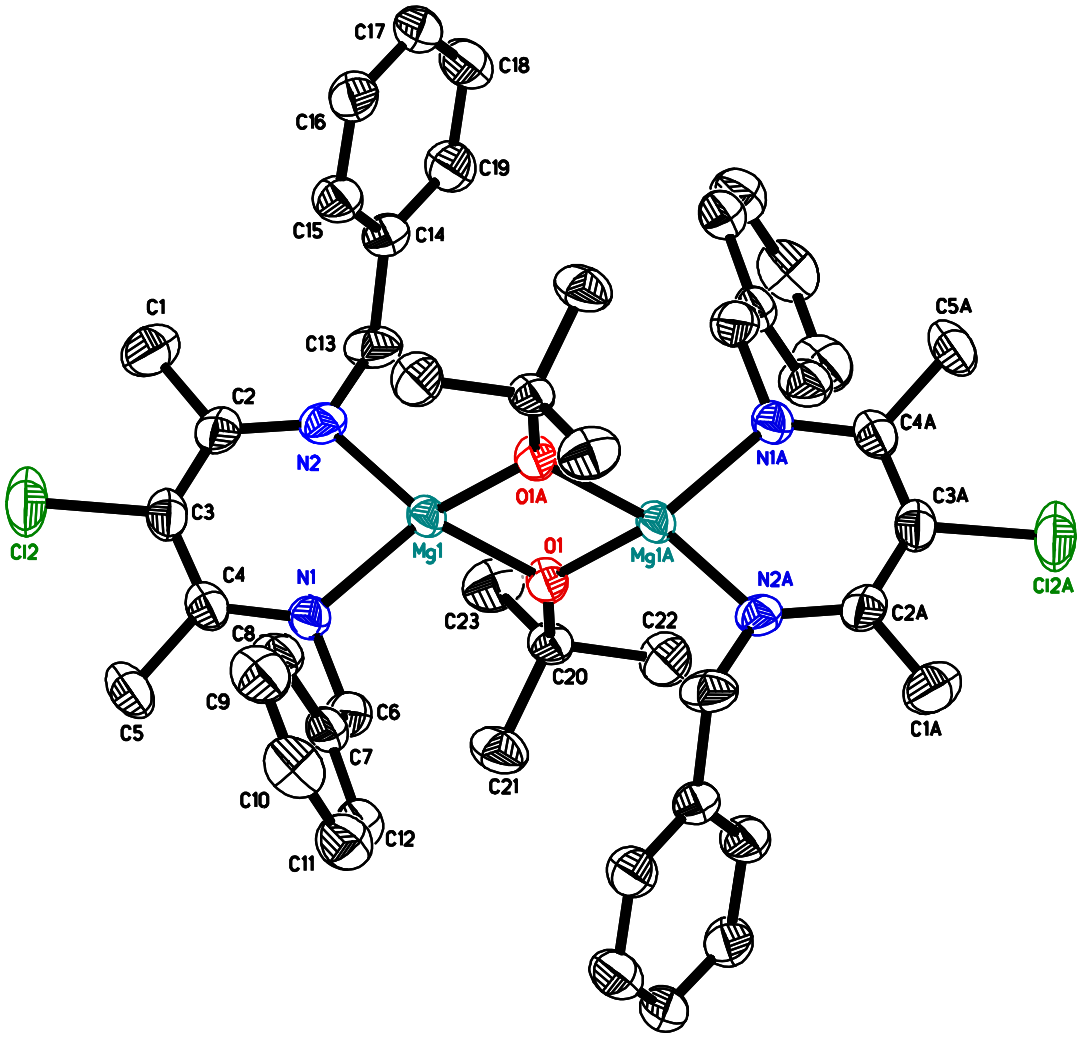

Fig. 8. X-ray structure of **6e**. Hydrogen atoms omitted for clarity. Thermal ellipsoids are drawn at 50% probability. Bond distances/Å: Mg1-N1: 2.035(2), Mg1-N2: 2.038(2), Mg1-O1: 1.952(2), Mg1-O1A: 1.964(2), Mg1-Mg1A: 2.915(1). Bond angles/deg: N1-Mg1-N2: 91.92(8), O1-Mg1-O1A: 83.79(7), N1-Mg1-O1: 125.38(8), N1-Mg1-O1A: 116.45(8), N2-Mg1-O1: 122.26(8), N2-Mg1-O1A: 120.25(8).

Reactions of **8a** with magnesium amide mirror the reactivity observed for the non-chlorinated analog **5a** in that preparation of the amide complex **8d** was straightforward, but we were unable to obtain an isolable alkoxide complex (Scheme 6). Single crystals were obtained for **8d**, but the obtained structure suffered from weak diffraction intensities and the presence of two independent molecules, one of which was severely disordered. We thus refrain from a discussion of this structure, the overall geometry of which is very similar to that of **5d**.[61] A single crystal of the homoleptic bis(diketiminate) complex, (Cl-*nacnac*^{An})$_2$Mg, **8f**, was obtained as a minor byproduct with clearly different morphology in one

recrystallisation of **8d**. The structure of **8f** (Fig. 9) shows π-stacking interactions between the anthryl moiety and the chloro-diketiminate backbone for two anthrylmethyl substituents, while the remaining two are in a coplanar arrangement with each other. Mg-N bond distances in **8f** are slightly longer by 0.04° and N-Mg-N bite angles are slightly smaller by 2° than in the respective *N*-benzyl complex **6f** (Table 3), indicating some small increase in steric bulk. It should be noted, however, that replacing phenyl by anthryl seems to have only a minor steric impact, comparable to that of chlorination of the β-position.

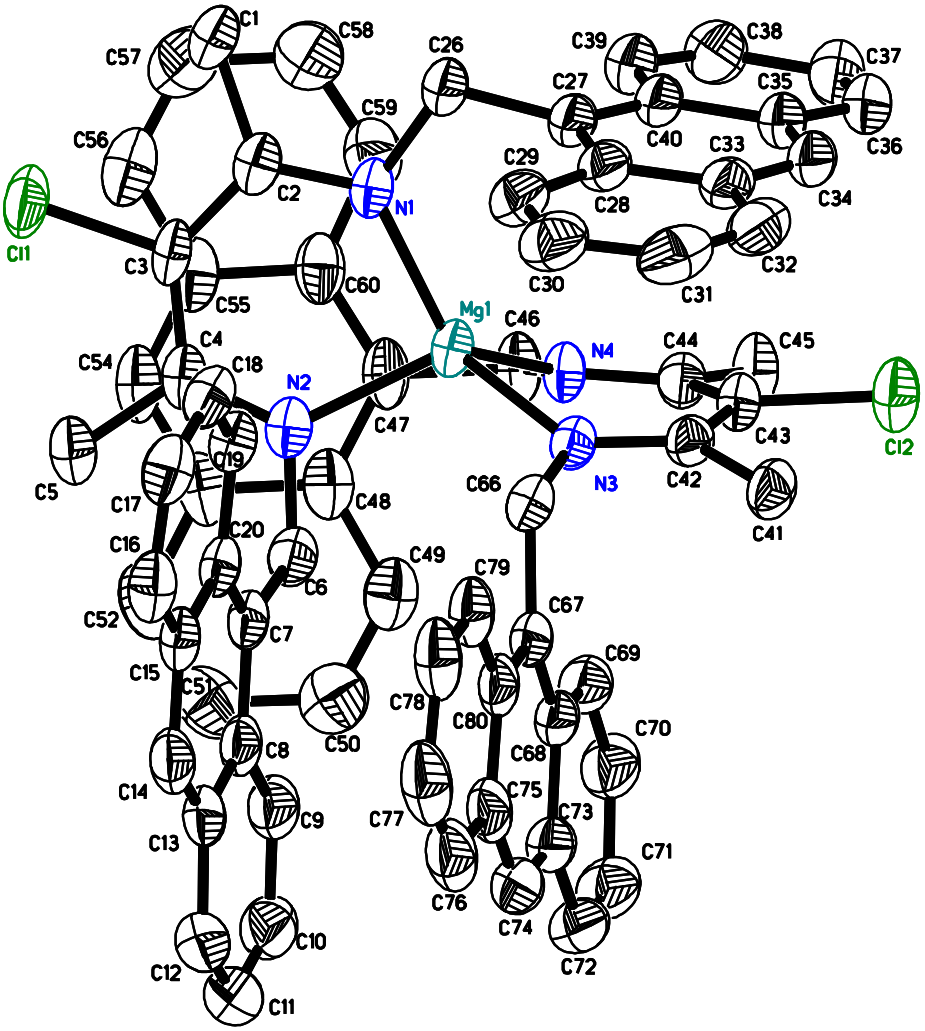

Fig. 9. X-ray structure of **8f**. Hydrogen atoms omitted for clarity. Thermal ellipsoids are drawn at 50% probability. Bond distances/Å: Mg-N: 2.065(2) – 2.076(2). Bond angles/deg: N1-Mg1-N2: 88.04(7), N3-Mg1-N4: 87.20(7), N_{Lig1}-Mg1-N_{Lig2}: 108.30(8) – 128.65(7).

In the absence of an isolable alkoxide complex, lactide polymerization was again performed with the amide complex **8d** in the presence of benzyl alcohol. An activity lower than that of **5d**/BnOH, significant catalyst decomposition and an uninteresting P_r-value of 0.48 were observed (Table 2, #15; Fig. S9). Polymerizations with **8d**/BnOH were thus not investigated further. Complex **6e**, on the other hand, was very active in lactide polymerization, reaching conversions above 70 – 80% after 10 min (Table 2, #12-#14). As for **3**, a notable induction period was observed in conversion vs. time plots which, accompanied by broadened polydispersities, indicated slow initiation through insertion into the Mg-O*t*Bu bond (Fig. S10). Addition of benzyl alcohol removed the induction period and narrowed polydispersities to 1.0 – 1.2 (Fig. S10). However, observed activities, number of polymer chains obtained per Mg and final conversions varied widely, the latter being as low as 30%. This indicates that *tert*-butanol, liberated by reaction with BnOH, remained active as a chain transfer reagent and that catalyst decomposition occurs in the presence of free alcohol. Side reactions can be suppressed by lowering the polymerization temperature to –30 °C, yielding reproducible results, polydispersities of 1.1 and only one polymer chain per metal center.

While **6e**, as **3**, has a slight heterotactic bias at room temperature (P_r = 0.54), addition of benzyl alcohol inexplicably reduced the P_r value to 0.46 – 0.49. Chain-transfer reactions due to the free alcohol present should not affect stereoselectivity in the case of a highly flexible ligand. However, catalyst decomposition (indicated by the lack of complete conversion) might yield species which are polymerization-active, but lack the slight heterotacticity of **6e**. Alternatively, decomposition products might be capable to catalyze transesterification to a higher degree than **6e**, which would lower the apparent P_r, since the statistical method used for its calculation does not allow the presence of rr-triads.[22] Lowering the polymerization temperature to –30 °C reduced P_r to 0.43, which is a slightly higher isotactic preference than observed for **3** under the same conditions (P_r = 0.46). Since chain transfer and catalyst decomposition are absent at this temperature, this reflects a small, but reproducible isotactic preference of **6e**, the highest observed so far for a diketiminate complex.

Conclusions

For Zn-based diketiminate catalysts, the flexible ligand framework provided by *N*-CH_2R substituents does not seem to offer a significant advantage in polymerization performance. As observed for the more rigid *N*-aryl substituents, activities in *rac*-lactide polymerization decrease with increasing substitution of the diketimine,[23, 24, 26, 28-30, 37] and the activity of sterically demanding **6c** ($k_p \approx 0.1$ $M^{-1}{\cdot}s^{-1}$) is at the lower end of the range obtained with *N*-alkyl substituted diketimines ($k_p \approx 0.1 - 0.5$ $M^{-1}{\cdot}s^{-1}$).[22] Stereoselectivities follow the general trend for Zn diketiminate complexes: a heterotactic preference reinforced by sterically demanding ligands.

For magnesium complexes, on the other hand, *N*-alkyl diketiminate ligands showed significant improvements when compared to their more rigid *N*-aryl analogues. With bulky **5d**, complete conversion of monomer was achieved in less than one minute ($k_p \approx 50$ $M^{-1}{\cdot}s^{-1}$), faster than its analogue with the sterically bulky 2,6-diisopropylphenyl substituent ($k_p = 11$ $M^{-1}{\cdot}s^{-1}$) and thus one of the fastest magnesium based catalysts reported.[42] Even more importantly, the isotactic preference previously observed for **3** was again obtained (slightly increased) in its chlorinated analogue **6e**. This is in contrast to the respective *N*-aryl complexes which display slight to strong heterotactic preferences. The reversal of stereopreference might be associated with the ability of the ligand framework to adapt itself to the last inserted monomer unit.[62] The few Mg complexes which show isotactic preference for lactide insertion all contain tridentate ligands, which require partial dissociation prior to lactide coordination and might thus offer a similar degree of ligand flexibility.[45-47] However, significant increases in stereoselectivity will be required to enable us to investigate a potential mechanistic relationship between ligand flexibility and stereocontrol.

Experimental part

General. All reactions were carried out using Schlenk and glove box techniques under a nitrogen atmosphere. *Nacnac*^{Bn}H was prepared according to literature,[48, 63] as was (9-anthryl)methylamine,[64]

acetyl acetone ethylene glycol monoketal,[51] and $Zn(N(SiMe_3)_2)_2$.[65] Solvents were dried by passage through activated aluminum oxide (MBraun SPS), de-oxygenated by repeated extraction with nitrogen, and stored over molecular sieves. C_6D_6 was dried over sodium and degassed by three freeze-pump-thaw cycles. $CDCl_3$ and CD_2Cl_2 were dried over 3 Å molecular sieves. *rac*-Lactide (98%) was purchased from Sigma–Aldrich, purified by 3x recrystallisation from dry ethyl acetate and kept at –30 °C. All other chemicals were purchased from common commercial suppliers and used without further purification. ^1H and ^{13}C NMR spectra were acquired on a Bruker AVX 400 spectrometer. The chemical shifts were referenced to the residual signals of the deuterated solvents (C_6D_6: ^1H: d 7.16 ppm, ^{13}C: d 128.38 ppm, $CDCl_3$: ^1H: d 7.26 ppm, CD_2Cl_2: ^1H: d 5.32 ppm). Elemental analyses were performed by the Laboratoire d'analyse élémentaire (Université de Montréal). Molecular weight analyses were performed on a Waters 1525 gel permeation chromatograph equipped with three Phenomenex columns and a refractive index detector at 35 °C. THF was used as the eluent at a flow rate of 1.0 $mL \cdot min^{-1}$ and polystyrene standards (Sigma–Aldrich, 1.5 $mg \cdot mL^{-1}$, prepared and filtered (0.2 mm) directly prior to injection) were used for calibration. Obtained molecular weights were corrected by a Mark-Houwink factor of 0.58.[66]

***N,N'*-di(9-anthrylmethyl)-2-amino-4-imino-2-pentene, *nacnac*^{An}H, 5a.** In a sealed vessel acetylacetone ethylene glycol monoketal (0.70 g, 4.39 mmol) and (9-anthryl)methylamine (1.82 g, 8.79 mmol) were added. The vessel was closed and stirred at 110 °C for 4 hours or until the mixture had completely solidified. The solid was washed with cold diethyl ether, dried under reduced pressure and used for without further purification (1.30 g, 62%, 90% purity according to NMR).

^1H NMR (400 MHz, C_6D_6): δ 11.70 (s, 1H, NH), 7.88 (s, 2H, Ar), 7.68 (m, 8H, Ar), 7.09 (m, 4H, Ar), 6.81 (m, 4H, Ar), 4.73 (s, 5H, CH, NCH_2), 1.86 (s, 6H, CH_3). $^{13}C\{^1H\}$ NMR (100 MHz, C_6D_6): 194.3 (C=N), 131.5 (Ar), 131.2 (Ar), 130.1 (Ar), 128.0 (Ar), 127.3 (Ar), 125.2 (Ar), 124.5 (Ar), 124.4 (Ar), 94.9 ($HC(CN)_2$), 43.4 (NCH_2), 19.8 (Me). EI-HR-MS (*m*/*z*): calcd. for $C_{35}H_{30}N_2$ $[M+H]^+$: 479.2482; found: 479.2485.

The main contamination was the monocondensation product 4-(9-anthryl)methylamino-3-penten-2-one, *acnac*^{An}H, which was also the main product in unsuccessful condensation attempts described in the text. ^{1}H-NMR ($CDCl_3$, 400 MHz): δ 10.97 (s, 1H, NH), 8.48 (s, 1H, Ar), 8.20 (m, 2H, Ar), 8.01 (m, 2H, Ar), 7.57 (m, 2H, Ar), 7.48 (m, 2H, Ar), 5.37 (d, 2H, NCH_2), 5.05 (s, 1H, CH), 2.29 (s, 1H, CH_3), 1.90 (s, 1H, CH_3). $^{13}C\{^{1}H\}$ NMR (100 MHz, $CDCl_3$): 195.1 (C=O), 162.2 (C=N), 131.7 (Ar), 130.4 (Ar), 129.5 (Ar), 128.7 (Ar), 127.4 (Ar), 126.9 (Ar), 125.2 (Ar), 123.5 (Ar), 95.7 (H*C*CN), 39.8 (NCH_2), 28.9 (Me), 19.8 (Me). Anal. Calcd. for $C_{20}H_{19}NO$: C, 83.01; H, 6.62; N, 4.84. Found: C, 82.84; H, 6.54; N, 4.80.

***nacnac*^{An}ZnN(SiMe$_3$)$_2$, 5b. 5a** (0.34g, 0.71 mmol) was added to a solution of $Zn(N(SiMe_3)_2)_2$ (0.27 g, 0.71 mmol) in toluene or hexane in the glove box, forming a suspension. Stirring was continued for 4 days or until the mixture became homogeneous. Solvent and formed amine were removed under reduced pressure. The crude solid was used in further reactions without purification. Recrystallisation from toluene yielded analytically pure, colourless crystals (0.38 g, 76%).

^{1}H NMR (400 MHz, C_6D_6): 8.33 (s, 2H, Ar), 8.20(m, 8H, Ar), 7.91(m, 4H, Ar), 7.37(m, 4H, Ar), 5.54(s, 4H, NCH_2), 4.41(s, 1H, CH), 1.71 (s, 6H, Me), -0.59(s, 18H, $SiMe_3$). $^{13}C\{^{1}H\}$ NMR (100 MHz, C_6D_6): 169.5 (C=N), 131.9 (Ar), 131.7 (Ar), 130.4 (Ar), 129.4 (Ar), 127.9 (Ar), 126.0 (Ar), 124.9 (Ar), 124.8 (Ar), 96.2 (H*C*$(CN)_2$), 48.7 (NCH_2), 24.7 (Me), 4.6 ($SiMe_3$). Anal. Calcd. for $C_{41}H_{47}N_3Si_2Zn$: C, 70.01; H, 6.74; N, 5.97. Found: C, 69.72; H, 6.57; N, 5.73.

***nacnac*^{An}ZnO*i*Pr·CH$_2$Cl$_2$, 5c.** To a solution of **5b** (0.38 g, 0.54 mmol) in toluene (5 mL), isopropanol (41 μL, 0.54 mmol) was added and allowed to react for 3 hr during which time a white precipitate appeared. The solvent was removed under reduced pressure, yielding the crude product as a white solid. Purification was carried out by recrystallisation in dichloromethane (0.11 g, 34%).

^{1}H NMR (400 MHz, $CDCl_3$): 8.35 (m, 4H, Ar), 8.22(s, 2H, Ar), 7.82(m, 4H, Ar), 7.25 (m, 8H, Ar), 5.37 (s, 4H, NCH_2), 4.12 (s, 1H, CH), 3.89 (sept., 1H, C*H*Me_2), 1.39 (s, 6H, Me), 1.07 (d, 6H, CH*Me*$_2$). $^{13}C\{^{1}H\}$ NMR (100 MHz, $CDCl_3$): 169.4 (C=N), 133.4 (Ar), 131.6 (Ar), 130.3 (Ar), 129.1 (Ar), 127.1 (Ar), 125.6 (Ar), 125.4 (Ar), 124.7 (Ar), 94.3 (H*C*$(CN)_2$), 53.6 (*C*HMe_2), 49.5 (NCH_2), 28.1 (Me), 24.7

(Me). Anal. Calcd. for $C_{38}H_{36}N_2OZn{\cdot}CH_2Cl_2$: Anal. Calcd. for $C_{38}H_{36}N_2OZn$ (CH_2Cl_2): C, 68.18; H, 5.57; N, 4.08. Combustion Analysis, found: C, 68.08; H, 5.29; N, 4.10. (One equivalent of dichloromethane per Zn was also observed in the crystal structure of **5c**.)

***nacnac*^{An}MgN(SiMe$_3$)$_2$, 5d. 5a** (1.07 g, 2.2 mmol) was added to a solution of $Mg(N(SiMe_3)_2)_2$ (0.86g, 2.5 mmol) in toluene or hexane, forming a suspension. The mixture was allowed to stir overnight, after which solvent and formed amine were removed under reduced pressure. The crude solid could be used either directly for further reactions or recrystallized from toluene (colourless crystals, 1.21 g, 82%).

^{1}H NMR (400 MHz, C_6D_6): δ 8.27 (d, 4H, Ar), 8.11 (s, 2H, Ar), 7.76 (d, 4H, Ar), 7.27 (8H, Ar), 5.25 (s, 4H, NCH_2), 4.69 (s, 1H, CH), 1.83(s, 6H, (NC)Me), -0.50 (s, 18H, $SiMe_3$). $^{13}C\{^1H\}$ NMR (100 MHz, C_6D_6): δ 170.2 (C=N), 132.3 (Ar), 131.5 (Ar), 131.2 (Ar), 129.8 (Ar), 128.6 (Ar), 126.8 (Ar), 125.3 (Ar), 124.7 (Ar), 95.8 (CH), 47.9 (NCH_2), 24.1 ((NC)Me), 4.4 ($SiMe_3$). Anal. Calcd. for $C_{41}H_{47}MgN_3Si_2$: C, 74.35; H, 7.15; N, 6.34. Found C, 74.45; H, 7.25; N, 6.20.

***nacnac*^{An}MgO*t*Bu, 5e.** A solution of **5d** in C_6D_6 was slowly titrated with a solution of *tert*-butanol in C_6D_6. After addition of 0.25 equiv the solution contained **5d** and **5e**. ^{1}H-NMR (C_6D_6, 400 MHz): δ 8.82 (d, 4H Ar), 8.24 (d, 4H Ar), 8.20 (s, 2H Ar), 8.10 (s, 2H Ar), 7.82 (d, 4H Ar), 7.76 (d, 4H Ar), 5.80 (s, 4H, NCH_2), 4.43 (s, 1H, CH), 1.53 (s, 6H, (NC)Me), 1.10 (s, 9H, $OCMe_3$). Further addition of *tert*-butanol led to the formation of the ligand **5a** and unidentified side-products.

***N,N'*-dibenzyl-2-amino-3-chloro-4-imino-2-pentene, Cl*nacnac*^{Bn}H, 6a.** To a solution of *nacnac*^{Bn}H (5.48 g, 19.7 mmol) in dry THF (150 mL) was added *N*-chlorosuccinimide (3.00 g, 22.4 mmol). After stirring at room temperature for 45 minutes, a white precipitate formed, which was removed by filtration. H_2O (500 mL) was then added. The product was extracted using hexanes (2 x 600 mL). After drying over Na_2SO_4, the solvent was evaporated. The obtained yellow oil was crystallized from dry ethanol at –80 °C, washed with cold dry ethanol and recrystallized from refluxing ethanol. The eluate yielded a second fraction at –80 °C (colourless crystals, 3.41 g, 55%).

^{1}H-NMR ($CDCl_3$, 400 MHz, 298 K): δ 12.22 (bs, 1H, NH), 7.25-7.19 (m, 10H, Ph), 4.49 (s, 4H, NCH_2), 2.18 (s, 6H, Me). $^{13}C\{^1H\}$ NMR ($CDCl_3$, 75 MHz, 298 K): δ 160.3 (*C*=N), 140.5 (*ipso* Ph),

128.6 (*ortho* or *meta* Ph), 127.3 (*ortho* or *meta* Ph), 126.8 (*para* Ph), 127.7 (ClC), 51.5 (NCH_2), 17.3 (Me). Anal. Calcd. for $C_{19}H_{21}ClN_2$: C, 72.95; H, 6.77; N, 8.95. Found C, 72.89; H, 6.66; N, 9.17.

Cl*nacnac*^{Bn}ZnO*i*Pr, 6c. $Zn(N(SiMe_3)_2)_2$ (0.86 g, 2.2 mmol) was added to a solution of **6a** (0.70 g, 2.2 mmol) in toluene (30 mL) over 5 min. The solvent was removed under reduced pressure, yielding Cl*nacnac*^{Bn}ZnN$(SiMe_3)_2$, **6b**, as an orange oil (1.25g, 2.21 mmol, ^{1}H NMR (400 MHz, C_6D_6): 7.22-7.14 (m, 10H, Ph), 4.85 (s, 4H, NCH_2), 2.21 (s, 6H, $Me(C{=}N)_2$), 0.20 (s, 18H, $SiMe_3$).

Toluene (30 mL), followed by isopropanol (0.13 g, 2.20 mmol) were added. After 5 min of stirring, a white precipitate formed, which was isolated by filtration and washed with toluene (15 mL). 0.30 g, 26%.

^{1}H NMR (400 MHz, C_6D_6): δ 7.16-7.05 (m, 10H, Ph), 4.57 (s, 4H, NCH_2), 3.85 (sep., 1H, $OC(H)Me_2$), 2.11 (s, 6H, $Me(C{=}N)_2$), 0.96 (d, 6H, $OC(H)Me_2$). ^{13}C{^{1}H} NMR (75 MHz, C_6D_6): δ 169.5 (C=N), 140.6 (Ph), 128.3 (Ph), 126.5 (Ph), 126.4 (Ph), 101.2 (Cl*C*), 66.2 ($OCHMe_2$ or NCH_2), 55.0 ($OCHMe_2$ or NCH_2), 27.9 (Me) 20.8 (Me). Anal. Calcd. for $C_{22}H_{27}ClN_2OZn$: C, 60.56; H, 6.24; N, 6.42. Found C, 60.10; H, 6.21; N, 6.35.

Cl*nacnac*^{Bn}MgO*t*Bu, 6e. To a solution of **6a** (0.100 g, 0.32 mmol) in anhydrous THF (6 mL), $Mg(N(SiMe_3)_2)_2$ (0.110 g, 0.32 mmol) was added. The yellow-golden solution was stirred overnight followed by solvent evaporation under reduced pressure yielding a yellow solid; identified as a mixture of Cl*nacnac*^{Bn}MgO*t*Bu, **6d**, and (Cl*nacnac*^{Bn})$_2$Mg, **6f.** After re-dissolution in THF (6 mL), *tert*-butanol (0.024 g, 0.32 mmol) was added. The reaction mixture was stirred for 3 hours. Evaporating the solvent yielded a yellow solid, which was washed with hexane and dried under reduced pressure. Recrystallisation from CH_2Cl_2/hexane at room temperature afforded colourless crystals after 24 h (0.04 g, 33%).

^{1}H-NMR (C_6D_6, 400 MHz): δ 7.35-6.95 (m, 10H, Ph), 4.68 (s, 4H, NCH_2), 2.19 (s, 6H, (NC)Me), 0.91 (s, 9H, $OCMe_3$). ^{13}C{^{1}H} NMR (100 MHz, C_6D_6): δ 170.6 (*C*=N), 141.0 (*ipso* Ph), 128.7 (*ortho* or *meta* Ph), 128.1 (*ortho* or *meta* Ph), 127.8 (*para* Ph), 126.7 (CCl), 67.5 ($OCMe_3$), 53.5 (NCH_2), 33.8

(OC*Me*$_3$), 20.9 ((NC)*Me*). Anal. Calcd. for $C_{23}H_{29}ClMgN_2O$: C, 67.50; H, 7.14; N, 6.85. Found C, 66.28; H, 7.28; N, 6.74.

(Cl*nacnac*^{Bn})$_2$Mg, 6f. To a solution of **6a** (0.100 g, 0.32 mmol) in anhydrous toluene (5 mL), Mg(N(SiMe$_3$)$_2$)$_2$ (0.055 g, 0.16 mmol) was added. The yellow-golden solution was stirred overnight. After evaporation of the solvent, the product, a bright solid, was identified by NMR spectroscopy. The obtained solid was re-dissolved in a minimum of toluene and crystallized at -35 °C to yield yellow crystals (0.09 g, 91%).

^{1}H-NMR (C_6D_6, 400 MHz): δ 7.28-6.89 (m, 20H, Ph), 4.15 (s, 8H, NCH_2), 2.05 (s, 12H, Me). $^{13}C\{^1H\}$ NMR (100 MHz, C_6D_6): δ 169.3 (C=N), 140.9 (*ipso* Ph), 128.5 (*ortho*/*meta* Ph), 128.1 (*ortho*/*meta* Ph), 126.8 (*para* Ph), 126.6 (CCl), 53.3 (NCH_2), 20.1 (Me). Anal. Calcd. for $C_{38}H_{40}Cl_2MgN_4$: C, 70.44; H, 6.22; N, 8.65. Found C, 70.33; H, 6.37; N, 8.48.

***N,N'*-di(mesitylmethyl)-2-amino-4-imino-2-pentene, *nacnac*^{Mes}H, 7a.** In a sealed vessel with a stir bar, acetylacetone ethylene glycol monoketal (0.19 g, 1.68 mmol) and mesitylmethylamine (0.5 g, 3.35 mmol) were added along with activated 3Å molecular sieve. The vessel was closed and heated to 110 ^oC for 4 hours or until the reaction had completely solidified. The solid product was dissolved in ethanol and crystallized (0.32 g, 52%).

^{1}H NMR (400 MHz, C_6D_6): 11.17 (s, 1H, NH), 6.72 (s, 4H, Ar), 4.63 (s, 1H, CH), 4.10 (s, 4H, NCH_2), 2.28 (s, 6H, ArC*H*$_3$), 2.00 (s, 12H, ArC*H*$_3$), 1.80 (s, 6H, CH_3). $^{13}C\{^1H\}$ NMR (100 MHz, C_6D_6): 159.9 (C=N), 136.8 (*ipso* Mes), 135.5 (*ortho/meta* Mes), 134.3 (*ortho/meta* Mes), 129.2 (*para* Mes), 94.7 (H*C*(CN)$_2$), 44.9 (NCH_2), 21.2 (Me), 19.5 (Me), 19.4 (Me). Anal. Calcd. for $C_{25}H_{42}N_2$: C, 82.82; H, 9.45; N, 7.73. Found C, 82.84; H, 9.46; N, 7.89.

***nacnac*^{Mes}MgN(SiMe$_3$)$_2$, 7d.** Following the procedure described for **5d**, **7a** (0.30 g, 0.83 mmol), Mg(N(SiMe$_3$)$_2$)$_2$ (0.29 g, 0.83 mmol) to yield colourless crystals (0.17 g, 37%).

^{1}H NMR (400 MHz, C_6D_6): δ 6.74 (s, 4H, Ar), 4.64 (s, 1H, CH), 4.28 (s, 4H, NCH_2), 2.28 (s, 6H, CN)Me), 2.09 (s, 12H, ArMe), 1.80 (s, 6H, ArMe) 0.00 (s, 18H, $SiMe_3$). $^{13}C\{^1H\}$ NMR (75 MHz, C_6D_6): δ 169.7 (C=N), 137.1 (Ar), 137.0 (Ar), 134.3 (Ar), 130.4 (Ar), 95.1 (CH), 48.8 (NCH_2), 23.4

(Me), 20.9 (Me), 20.7 (Me), 4.6 ($SiMe_3$). Anal. Calcd. for $C_{31}H_{51}MgN_3Si_2$: C, 68.16; H, 9.41; N, 7.69. Found .23 ; H, 9.50; N, 7.70.

***nacnac*^{Mes}MgO*t*Bu·½CH_2Cl_2, 7e.** As in **5c**, substituting **5b** for **7d** (0.13 g, 0.24 mmol), isopropanol for *tert*-butanol (23 µL, 0.24 mmol). Colourless crystals after recrystallisation from dichloromethane (72 mg, 66%).

^{1}H-NMR (400 MHz, C_6D_6): δ 6.82 (s, 4H, Ar), 4.85 (s, 4H, NCH_2), 4.67 (s, 1H, CH), 2.48 (s, 12H, Ar*Me*), 2.16 (s, 6H, (CN)Me), 1.82 (s, 6H, Ar*Me*), 1.06 (s, 9H, $OCMe_3$). $^{13}C\{^1H\}$ NMR (100 MHz, C_6D_6): δ 169.9 (C=N), 136.5 (*ipso* Mes), 135.7 (*ortho/meta* Mes), 135.3 (*ortho/meta* Mes), 130.5 (*para* Mes), 80.9 (CH), 67.2 ($OC(CH_3)_3$), 44.9 (NCH_2), 33.1 (Me, *ortho*), 23.5 (Me, *para*), 21.6 ($OCMe_3$), 20.9 (NC*Me*). Anal. Calcd. for $C_{29}H_{42}MgN_2O·½CH_2Cl_2$: C, 70.66; H, 8.64; N, 5.59. Found 69.65; H, 8.68; N, 5.68. (Half an equivalent of CH_2Cl_2 per Mg was observed in the crystal structure.)

***N,N'*-di(9-anthrylmethyl)-2-amino-3-chloro-4-imino-2-pentene, Cl*nacnac*^{An}H, 8a.** To a solution of **5a** (1.00 g, 2.1 mmol) in anhydrous THF (40 mL) was added *N*-chlorosuccinimide (0.30 g, 2.3 mmol). After stirring at room temperature for 45 minutes, a white precipitate formed, which was removed by filtration. Water was then added. The product was extracted using dichloromethane (2 x 10 mL) and dried over Na_2SO_4. Evaporation of the solvent yielded a yellow oil, which was crystallized from anhydrous dichloromethane (0.45 g, 42%).

^{1}H NMR (400 MHz, C_6D_6): 12.32 (s, 1H, NH), 7.76 (s, 2H, Ar), 7.56 (m, 8H, Ar), 7.06 (m, 4H, Ar), 6.87 (m, 4H, Ar), 4.57 (s, 5H, CH, NCH_2), 2.12 (s, 6H, Me). $^{13}C\{^1H\}$ NMR (100 MHz, C_6D_6): 159.6 (C=N), 131.1 (Ar), 129.8 (Ar), 129.1(Ar), 127.5 (Ar), 125.3 (Ar), 125.1 (Ar), 124.4 (Ar), 124.0 (Ar), 100.6 (CCl), 44.1 (NCH_2), 17.2 (Me). Anal. Calcd. for $C_{35}H_{29}ClN_2$: C, 81.93; H, 5.70; N, 5.46. Found C, 81.73; H, 5.70; N, 5.47.

Cl*nacnac*^{An}MgN(SiMe$_3$)$_2$, 8d. Following the procedure described for **5d**, **5a** (0.12g, 0.23 mmol), $Mg(N(SiMe_3)_2)_2$ (0.08 g, 0.23 mmol), (crude 0.14 g, 87%) colourless crystals (0.05 g, 28%).

^{1}H NMR (400 MHz, C_6D_6): δ 8.13 (s, 2H, Ar), 8.10 (d, 4H, Ar), 7.75 (d, 4H, Ar), 7.31-7.21 (m, 8H, Ar), 5.16 (s, 4H, NCH_2), 2.31 (s, 6H, (NC)Me), -0.57 (s, 18H, $SiMe_3$). $^{13}C\{^1H\}$ NMR (100 MHz,

C_6D_6): δ 169.3 (C=N), 132.2 (Ar), 131.2 (Ar), 130.5 (Ar), 129.9 (Ar), 129.1 (Ar), 127.0 (Ar), 125.4 (Ar), 124.4 (Ar), 102.4 (Cl*C*$(CN)_2$), 48.9 (NCH_2), 21.4 (Me), 4.4 ($SiMe_3$). Anal. Calcd. for $C_{41}H_{46}ClMgN_3Si_2$: C, 70.68; H, 6.65; N, 6.03. Found C, 71.27; H, 6.47; N, 5.71.

X-ray diffraction studies. Single crystals were obtained as described in table S4. Diffraction data were collected with Cu Kα radiation on a Bruker Smart 6000 or a Bruker Microstar/Proteum, both equipped with Helios MX mirror optics and rotating anode sources, or on a Bruker Microsource/APEX2 using the APEX2 software package.[67] Data reduction was performed with SAINT,[68] absorption corrections with SADABS.[69] Structures were solved with direct methods (SHELXS97).[70] All non-hydrogen atoms were refined anisotropic using full-matrix least-squares on F^2 and hydrogen atoms refined with fixed isotropic U using a riding model (SHELXL97).[70] In **8f**, disordered solvent was found around the inversion center (93 electrons/unit cell), but the best modeled solution remained 12% higher in wR_2 (with appr. twice as high errors in bond lengths) than the solution after application of SQUEEZE. No notable structural difference was found between solutions and thus the latter was used. Further experimental details can be found in Table 4 and in the supporting information (CIF).

Table 4 Details of X-ray Diffraction Studies

	5b	**5c**	**5d**	**5f**	**6e**
Formula	$C_{41}H_{47}N_3Si_2Zn \cdot C_7H_8$	$C_{76}H_{72}N_4O_2Zn_2 \cdot 2\ CH_2Cl_2$	$C_{41}H_{47}MgN_3Si_2 \cdot 2\ CH_2Cl_2$	$C_{82}H_{68}Mg_2N_4O_2 \cdot 2.5\ CH_2Cl_2$	$C_{46}H_{58}Cl_2Mg_2N_4O_2$
M_w (g/mol); $d_{calcd.}$ (g/cm^3)	795.50; 1.246	1373.97; 1.387	747.23; 1.224	1402.33; 1.314	818.48; 1.236
Crystal size (mm)	0.15·0.15·0.18	0.27·0.27·0.36	0.16·0.09·0.09	0.18·0.14·0.11	0.14·0.14·0.14
T (K); F(000)	150; 1688	150; 716	200; 792	100; 1466	150; 872
Crystal System	Triclinic	Triclinic	Triclinic	Triclinic	Monoclinic
Space Group	P-1	P-1	P-1	P-1	$P2_1/c$
Unit Cell: a (Å)	13.0063(3)	11.8196(4)	11.4629(5)	14.4200(5)	9.1499(2)
b (Å)	15.7472(4)	12.4402(5)	12.8758(6)	16.6394(6)	22.1705(3)
c (Å)	20.9693(5)	12.4806(5)	14.0056(6)	17.0800(6)	10.8809(2)
α (°)	84.7981(11)	95.050(1)	92.665(3)	72.642(2)	
β (°)	86.8527(12)	115.269(2)	98.376(3)	73.431(2)	95.103(1)
γ (°)	83.0374(10)	92.814(1)	96.507(3)	67.467(2)	
V (Å^3); Z	4241.4(2); 4	1645.4(1); 1	2027.74(16); 2	3544.4(2); 2	2198.53(7); 2
θ range (°); completeness	2-73; 0.96	4-72; 0.95	3-73; 0.96	3-73; 0.96	4-73; 0.97
collected reflections; R_σ	56188; 0.026	21587; 0.021	26826; 0.070	47715; 0.039	28207; 0.038
unique reflections; R_{int}	16111; 0.034	6223; 0.035	7708; 0.089	13541; 0.035	4271; 0.072
μ (mm^{-1}); Abs. Corr.	1.246; multiscan	2.790; multiscan	2.402; multiscan	2.447; multiscan	1.926; multiscan
R1(F); wR(F^2) (I > 2σ(I))	0.040; 0.114	0.046; 0.114	0.054; 0.144	0.049; 0.138	0.058; 0.155
R1(F); wR(F^2) (all data)	0.045; 0.118	0.047; 0.115	0.070; 0.153	0.062; 0.147	0.066; 0.183
GoF(F^2)	0.91	0.86	1.01	1.08	1.15
Residual electron density	1.08; -0.73	0.57; -0.80	0.71; -0.55	0.41; -0.42	0.47; -0.72

	6f	**7d**	**7e**	**8f**
Formula	$C_{38}H_{40}Cl_2MgN_4$	$C_{31}H_{51}MgN_3Si_2$	$C_{29}H_{43}MgN_2O \cdot 0.5\ CH_2Cl_2$	$C_{70}H_{56}Cl_2MgN_4$
M_w (g/mol); $d_{calcd.}$ (g/cm^3)	647.9; 1.290	546.24; 1.111	501.42; 1.167	1048.39; 1.224
Crystal size (mm)	0.18·0.16·0.16	0.14·0.11·0.07	0.15·0.15·0.15	0.13·0.08·0.08
T (K); F(000)	150; 1368	100; 1192	100; 2168	100; 1100
Crystal System	Monoclinic	Orthorhombic	Monoclinic	Triclinic
Space Group	$P2_1/c$	$Pnma$	$P2_1/n$	P-1
Unit Cell: a (Å)	14.5416(5)	17.4882(2)	15.0133(8)	12.5041(8)
b (Å)	11.1177(4)	18.0767(2)	17.0252(9)	14.3017(8)
c (Å)	20.7327(7)	10.3297(1)	22.8695(13)	18.1609(10)
α (°)				104.305(2)
β (°)	95.640(2)		102.436(2)	109.464(2)
γ (°)				100.227(2)
V (Å^3); Z	3335.6(2); 4	3265.52(6); 4	5708.4(5); 8	2844.6(3); 2
θ range (°); completeness	3-73; 0.97	5-72; 0.98	3-72; 0.99	3-58; 0.98
collected reflections; R_σ	40209; 0.021	45504; 0.011	80320; 0.026	52174; 0.046
unique reflections; R_{int}	6473; 0.037	3233; 0.025	11142; 0.042	7765; 0.029
μ (mm^{-1}); Abs. Corr.	2.185; multiscan	1.334; multiscan	1.567; multiscan	1.484; multiscan
R1(F); wR(F^2) ($I > 2\sigma(I)$)	0.039; 0.107	0.034; 0.095	0.054; 0.150	0.048; 0.136
R1(F); wR(F^2) (all data)	0.043; 0.111	0.035; 0.096	0.059; 0.155	0.051; 0.139
GoF(F^2)	1.05	1.06	1.05	1.04
Residual electron density	0.28; -0.43	0.40; -0.28	1.01; -0.71	0.30; -0.52

Acknowledgements. Johannes T. Wendler's, Simon Cassegrain's and Marine Cros' contributions to these studies during their internships are gratefully acknowledged. We thank F. Bélanger for support with X-ray diffraction studies and Prof. R. E. Prud'homme and P. Ménard-Tremblay for access to GPC. Funding was provided by NSERC, Centre en chimie verte et catalyse (CCVC) and FQRNT (Ph. D. stipend for T. W.).

Supporting Information. Tables S1-S4. Lactide conversion/time plots (Fig. S1-S10). Single-crystal diffraction data (CIF).

1. R. G. Patel and D. J. Sen, *Int. Pharm. Sciencia*, 2011, **1**, 29.
2. K. Kishan and S. Carmen, in *Degradable Polymers and Materials: Principles and Practice (2nd Edition)*, American Chemical Society, 2012, vol. 1114, pp. 3-10.
3. G. E. Luckachan and C. K. S. Pillai, *J. Polym. Environ.*, 2011, **19**, 637–676.
4. R. C. Thompson, C. J. Moore, F. S. v. Saal and S. H. Swan, *Phil. Trans. R. Soc. B* 2009, **364**, 2153-2166.
5. J. Hammer, M. S. Kraak and J. Parsons, in *Reviews of Environmental Contamination and Toxicology*, ed. D. M. Whitacre, Springer New York, 2012, vol. 220, pp. 1-44.
6. D. K. A. Barnes, F. Galgani, R. C. Thompson and M. Barlaz, *Philos. Trans. R. Soc., B*, 2009, **364**, 1985-1998.
7. M. Cole, P. Lindeque, C. Halsband and T. S. Galloway, *Mar. Pollut. Bull.*, 2011, **62**, 2588-2597.
8. C. K. Williams and M. A. Hillmyer, *Polym. Rev.*, 2008, **48**, 1-10.
9. J. Ahmed and S. K. Varshney, *International Journal of Food Properties*, 2011, **14**, 37-58.
10. S. Inkinen, M. Hakkarainen, A.-C. Albertsson and A. Södergård, *Biomacromolecules*, 2011, **12**, 523-532.
11. S. Dutta, W.-C. Hung, B.-H. Huang and C.-C. Lin, in *Synthetic Biodegradable Polymers*, eds. B. Rieger, A. Künkel, G. W. Coates, R. Reichardt, E. Dinjus and T. A. Zevaco, Springer-Verlag, Berlin, 2011, pp. 219-284.
12. P. J. Dijkstra, H. Du and J. Feijen, *Polym. Chem.*, 2011, **2**, 520-527.
13. J.-F. Carpentier, *Macromol. Rapid Comm.*, 2010, **31**, 1696-1705.
14. N. Ajellal, J.-F. Carpentier, C. Guillaume, S. M. Guillaume, M. Helou, V. Poirier, Y. Sarazin and A. Trifonov, *Dalton Trans.*, 2010, **39**, 8363.
15. C. A. Wheaton, P. G. Hayes and B. J. Ireland, *Dalton Trans.*, 2009, 4832 - 4846.
16. R. H. Platel, L. M. Hodgson and C. K. Williams, *Polym. Rev.*, 2008, **48**, 11 - 63.
17. M. H. Chisholm and Z. Zhou, *J. Mater. Chem.*, 2004, **14**, 3081.
18. I. El-Zoghbi, T. J. J. Whitehorne and F. Schaper, *Dalton Trans.*, 2013, **42**, 9376 - 9387.
19. T. J. J. Whitehorne and F. Schaper, *Chem. Commun. (Cambridge, U. K.)*, 2012, **48**, 10334-10336.
20. T. J. J. Whitehorne and F. Schaper, *Inorg. Chem.*, 2013, **52**, 13612-13622.
21. F. Drouin, T. J. J. Whitehorne and F. Schaper, *Dalton Trans.*, 2011, **40**, 1396-1400.

22. F. Drouin, P. O. Oguadinma, T. J. J. Whitehorne, R. E. Prud'homme and F. Schaper, *Organometallics*, 2010, **29**, 2139–2147.
23. M. Cheng, A. B. Attygalle, E. B. Lobkovsky and G. W. Coates, *J. Am. Chem. Soc.*, 1999, **121**, 11583-11584.
24. B. M. Chamberlain, M. Cheng, D. R. Moore, T. M. Ovitt, E. B. Lobkovsky and G. W. Coates, *J. Am. Chem. Soc.*, 2001, **123**, 3229-3238.
25. M. H. Chisholm, J. C. Huffman and K. Phomphrai, *J. Chem. Soc., Dalton Trans.*, 2001, 222-224.
26. M. H. Chisholm, J. Gallucci and K. Phomphrai, *Inorg. Chem.*, 2002, **41**, 2785-2794.
27. M. H. Chisholm and K. Phomphrai, *Inorg. Chim. Acta*, 2003, **350**, 121.
28. A. P. Dove, V. C. Gibson, E. L. Marshall, A. J. P. White and D. J. Williams, *Dalton Trans.*, 2004, 570-578.
29. M. H. Chisholm, J. C. Gallucci and K. Phomphrai, *Inorg. Chem.*, 2005, **44**, 8004-8010.
30. C. N. Ayala, M. H. Chisholm, J. C. Gallucci and C. Krempner, *Dalton Trans.*, 2009, 9237 - 9245.
31. R. Tong and J. Cheng, *Angew. Chem., Int. Ed.*, 2008, **47**, 4830-4834.
32. K. Yu and C. W. Jones, *J. Catal.*, 2004, **222**, 558.
33. K. Yu and C. W. Jones, *Polym. Prepr. (Am. Chem. Soc., Div. Polym. Chem.)*, 2004, **45**, 1005.
34. M. Kroeger, C. Folli, O. Walter and M. Doering, *Adv. Synth. Catal.*, 2006, **348**, 1908-1918.
35. M. Helou, O. Miserque, J.-M. Brusson, J.-F. Carpentier and S. M. Guillaume, *Macromol. Rapid Comm.*, 2009, **30**, 2128-2135.
36. V. Poirier, M. Duc, J.-F. Carpentier and Y. Sarazin, *ChemSusChem*, 2010, **3**, 579-590.
37. H.-Y. Chen, B.-H. Huang and C.-C. Lin, *Macromolecules*, 2005, **38**, 5400-5405.
38. T. Athar, A. Hakeem and N. Topnani, *J. Chil. Chem. Soc.*, 2011, **56**, 887-890.
39. H.-Y. Chen, Y.-L. Peng, T.-H. Huang, A. K. Sutar, S. A. Miller and C.-C. Lin, *J. Mol. Catal. A: Chem.*, 2011, **339**, 61-71.
40. L. F. Sanchez-Barba, D. L. Hughes, S. M. Humphrey and M. Bochmann, *Organometallics*, 2006, **25**, 1012-1020.
41. R. Tong and J. Cheng, *Bioconjugate Chem.*, 2010, **21**, 111-121.
42. M. H. Chisholm, K. Choojun, J. C. Gallucci and P. M. Wambua, *Chem. Sci.*, 2012, **3**, 3445-3457.
43. R. A. Collins, J. Unruangsri and P. Mountford, *Dalton Trans.*, 2013, **42**, 759-769.
44. Independent of their solid state structure, *nacnac*Zn(OR) complexes might be dimeric or monomeric in solution. Since solution structures of the (pre-)catalysts influence only the very first monomer insertion, they were not investigated in detail and all complexes are presented as monomers in the text to facilitate readability.
45. J.-C. Buffet, J. P. Davin, T. P. Spaniol and J. Okuda, *New J. Chem.*, 2011, **35**, 2253-2257.
46. L. Wang and H. Ma, *Macromolecules*, 2010, **43**, 6535-6537.
47. S. Song, H. Ma and Y. Yang, *Dalton Trans.*, 2013, **42**, 14200-14211.
48. I. El-Zoghbi, A. Ased, P. O. Oguadinma, E. Tchirioua and F. Schaper, *Can. J. Chem.*, 2010, **88**, 1040-1045.
49. J. Feldman, S. J. McLain, A. Parthasarathy, W. J. Marshall, J. C. Calabrese and S. D. Arthur, *Organometallics*, 1997, **16**, 1514-1516.
50. K. J. Fisher, *Tetrahedron Lett.*, 1970, 2613-2616.
51. J. Vela, L. Zhu, C. J. Flaschenriem, W. W. Brennessel, R. J. Lachicotte and P. L. Holland, *Organometallics*, 2007, **26**, 3416-3423.
52. M. Cheng, D. R. Moore, J. J. Reczek, B. M. Chamberlain, E. B. Lobkovsky and G. W. Coates, *J. Am. Chem. Soc.*, 2001, **123**, 8738-8749.
53. D. F. J. Piesik, S. Range and S. Harder, *Organometallics*, 2008, **27**, 6178-6187.
54. D. R. Moore, M. Cheng, E. B. Lobkovsky and G. W. Coates, *Angew. Chem., Int. Ed.*, 2002, **41**, 2599-2602.

55. R. Boese, D. Blaser, T. Eisenmann and S. Schulz, *Private communication to the Cambridge Structural Database*, 2009, CCDC 730654.
56. S. Schulz, T. Eisenmann, D. Bläser and R. Boese, *Z. Anorg. Allg. Chem.*, 2009, **635**, 995-1000.
57. G. Bendt, S. Schulz, J. Spielmann, S. Schmidt, D. Bläser and C. Wölper, *Eur. J. Inorg. Chem.*, 2012, 3725-3731.
58. A. P. Dove, V. C. Gibson, P. Hormnirun, E. L. Marshall, J. A. Segal, A. J. P. White and D. J. Williams, *Dalton Trans.*, 2003, 3088-3097.
59. S. Latreche and F. Schaper, *Inorg. Chim. Acta*, 2011, **43**, 49-53.
60. P. J. Bailey, R. A. Coxall, C. M. Dick, S. Fabre, L. C. Henderson, C. Herber, S. T. Liddle, D. Loroño-González, A. Parkin and S. Parsons, *Chem.-Eur. J.*, 2003, **9**, 4820-4828.
61. T. J. J. Whitehorne and F. Schaper, *Private Communication to the Cambridge Structural Database*, 2013, CCDC 972594.
62. H. Ma, T. P. Spaniol and J. Okuda, *Angew. Chem., Int. Ed.*, 2006, **45**, 7818-7821.
63. P. O. Oguadinma and F. Schaper, *Organometallics*, 2009, **28**, 6721–6731.
64. D. E. Stack, A. L. Hill, C. B. Diffendaffer and N. M. Burns, *Org. Lett.*, 2002, **4**, 4487-4490.
65. D. Rivillo, H. Gulyás, J. Benet-Buchholz, Eduardo C. Escudero-Adán, Z. Freixa and Piet W. N. M. van Leeuwen, *Angew. Chem., Int. Ed.*, 2007, **46**, 7247-7250.
66. M. Save, M. Schappacher and A. Soum, *Macromol. Chem. Phys.*, 2002, **203**, 889-899.
67. *APEX2*, (2006) Bruker AXS Inc., Madison, USA.
68. *SAINT*, (2006) Bruker AXS Inc., Madison, USA.
69. G. M. Sheldrick, *SADABS*, (1996 & 2004) Bruker AXS Inc., Madison, USA.
70. G. M. Sheldrick, *Acta Crystallogr.*, 2008, **A64**, 112-122.

Table of Contents

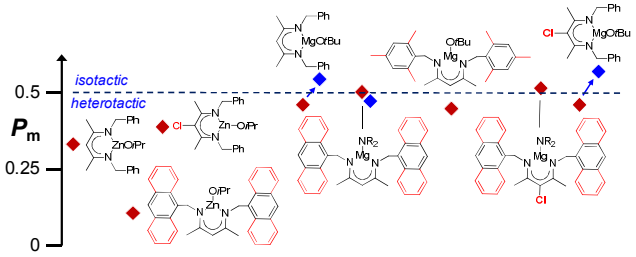

Subtle variations in the substitution pattern of *N*-alkyl diketiminate complexes significantly change their performance in lactide polymerization. Ortho-substitution increases activity, ligand chlorination increases selectivity for Mg diketiminate complexes, while Zn diketiminate complexes react differently.